Tectonophysics 710–711 (2017) 184–204

Contents lists available at ScienceDirect

Tectonophysics

journal homepage: www.elsevier.com/locate/tecto

Structure and provenance of Late Cretaceous–Miocene sediments located near the NE Dinarides margin: Inferences from kinematics of orogenic building and subsequent extensional collapse

Uros Stojadinovic [a,c,*], Liviu Matenco [b], Paul Andriessen [c], Marinko Toljić [a], Ljupko Rundić [a], Mihai N. Ducea [d,e]

[a] University of Belgrade, Faculty of Mining and Geology, Department of Regional Geology, Belgrade, Serbia
[b] Utrecht University, Faculty of Earth Sciences, Utrecht, The Netherlands
[c] VU University Amsterdam, Faculty of Earth and Life Sciences, Amsterdam, The Netherlands
[d] University of Arizona, Department of Geosciences, Tucson, AZ, USA
[e] University of Bucharest, Faculty of Geology and Geophysics, Bucharest, Romania

ARTICLE INFO

Article history:
Received 29 February 2016
Received in revised form 7 December 2016
Accepted 22 December 2016
Available online 28 December 2016

Keywords:
Low-exhumation orogens
Orogenic-driven extension
Detrital thermochronology
Provenance
Dinarides

ABSTRACT

The NE part of the Dinarides Mountain chain, located near their junction with the Carpatho-Balkanides, is an area where sedimentary basins associated with the Neotethys subduction and collision are still exposed. We performed a provenance study, based on detrital fission track thermochronology combined with zircon U—Pb magmatic geochronology, and existing studies of kinematics and exhumation. Our study shows rapid sedimentation in the trench and forearc basin overlying the upper European tectonic plate. A number of latest Cretaceous–Early Paleocene igneous provenance ages show a dominant magmatic source area, derived from a Late Cretaceous subduction-related arc. This arc shed short time lag sediments in the forearc and the trench system, possibly associated with focused exhumation in the Serbo-Macedonian margin. This was followed by burial of the trench sediments and a novel stage of Middle–Late Eocene exhumation driven by continued continental collision that had larger effects than previously thought. The collision was followed by Late Oligocene–Miocene exhumation of the former lower Adriatic plate along extensional detachments that reactivated the inherited collisional contact along the entire Dinarides margin. This event re-distributed sediments at short distances in the neighboring Miocene basins. Our study demonstrates that the Dinarides orogenic system is characterized by short lag times between exhumation and re-deposition, whereas the upper tectonic plate is significantly exhumed only during the final stages of collision. Such an exhumation pattern is not directly obvious from observing the overall geometry of the orogen.

1. Introduction

Orogens recording large amounts of shortening in the upper plate of the subduction/collision systems are generally associated with significant exhumation in their cores, resulting in the exposure of the deep lower crust by contractional mechanics. In such orogens, a wide range of thermochronological methods with various closure temperatures are used to derive kinematics, timing, exhumation and associated sedimentary basin evolution (e.g., Burov and Yamato, 2008; Erdos et al., 2015; Faccenda et al., 2009; Hatzfeld and Molnar, 2010; Naylor and Sinclair, 2008; Selzer et al., 2008; Willett and Brandon, 2002 and references therein). In contrast, orogenic building during periods of slab retreat is generally associated with reduced amounts of exhumation, the overall deformation being dominated by back-arc and/or forearc extension, orogenic collapse during subduction erosion and the evolution of associated sedimentary basins during shortening (Doglioni et al., 1999, 2007; Duretz and Gerya, 2013; Jammes and Huismans, 2012; Osmaston, 2008; Willingshofer and Sokoutis, 2009). In such settings, provenance studies in sedimentary basins yield indirect exhumation of source areas, residence and lag times, which are subsequently used to derive the first order controls of neighboring orogenic growth (Bernet and Spiegel, 2004a,b; Spiegel et al., 2000; von Eynatten and Dunkl, 2012). Such studies are important for example in the Mediterranean region, where numerous highly curved mountain belts formed during the slab-retreat of genetically associated subduction systems. There, the exhumation is locally difficult to discriminate between contraction or extension-driven (e.g., Carrapa et al., 2008;

* Corresponding author at: University of Belgrade, Faculty of Mining and Geology, Department of Regional Geology, Belgrade, Serbia.
E-mail address: uros.stojadinovic@rgf.bg.ac.rs (U. Stojadinovic).

http://dx.doi.org/10.1016/j.tecto.2016.12.021
0040-1951/

Faccenna et al., 2004; Reiners and Brandon, 2006). In such settings, the geometry and distribution of provenance ages in sedimentary basins provide first order constraints on the overall kinematics.

An excellent natural laboratory for the evolution of an orogen above a retreating slab is observed along NE margin of the Dinarides Mountains at their junction with the Carpatho-Balkanides (Fig. 1). The Dinarides experienced a long-lived Jurassic–Paleogene period of convergence by subduction of a SE European branch of the Neotethys Ocean. This was associated with obduction, continental collision and subsequent shortening between Adriatic (i.e. Dinarides) and European (i.e. Carpatho-Balkanides) derived continental units (Dimitrijević, 1997; Karamata, 2006; Robertson et al., 2009; Schmid et al., 2008). Intriguing are the stages of Late Cretaceous–Paleogene shortening that are associated at first with Late Cretaceous extension in the forearc and backarc domain, and with the emplacement of the Apuseni, Banat, Timok, Panagyurishte, and Eastern Srednogorie calk-alkaline magmatism (Fig. 1, e.g., Antić et al., 2015; Gallhofer et al., 2015; von Quadt et al., 2005). This was subsequently followed by the onset of a latest Cretaceous continental collision and the formation of the Sava suture zone (e.g., Pamić, 2002; Ustaszewski et al., 2009), followed by a continuation of contraction during Paleogene times (e.g., Tari, 2002). The contraction was associated with significant latest Cretaceous–Paleogene sedimentation in the trench, forearc or overlying various nappe contacts in the NE Dinarides (Fig. 1, e.g., Toljić et al., submitted for publication). Later yet, the onset of the Miocene back-arc extension of the Pannonian Basin (e.g., Horváth et al., 2015) resulted in the formation of a number of (half-)grabens filled with Miocene sediments and separated by the uplifted footwalls of extensional detachments (Figs. 1 and 2). These Miocene sediments largely covered the earlier orogenic structure (e.g., Čanović and Kemenci, 1988; Matenco and Radivojević, 2012), with the notable exception of large areas in the NE Dinarides. The overall structure and thermal overprint of the Miocene tectonics make discrimination of orogenic kinematics in direct exhumation studies difficult. Therefore, indirect methodologies, such as provenance studies, are required to understand the timing of events, exhumation and kinematics during the orogenic collision of the Dinarides.

In order to quantify the effects of the latest Cretaceous–Miocene orogenic build-up and extensional collapse, we performed an exhumation and provenance multi-dating approach that included zircon and apatite fission tracks (ZFT and AFT), combined with zircon U—Pb geochronology aimed at understanding the emplacement of a couple of critical plutons in the studied area (i.e. Bukulja and Cer granitoids, Figs. 1 and 2). These thermochronological measurements were combined with existing and new kinematic observations in the critical studied areas of Fruška Gora, Cer, Bukulja and Belgrade surroundings. A number of key sedimentary units were chosen in the study area that were considered diagnostic for sediment routing in Cretaceous and Miocene sediments located either in the Sava suture zone or in the hanging-wall of major Miocene detachments. Provenance, transport and lag times were derived by the correlation with existing studies of exhumation

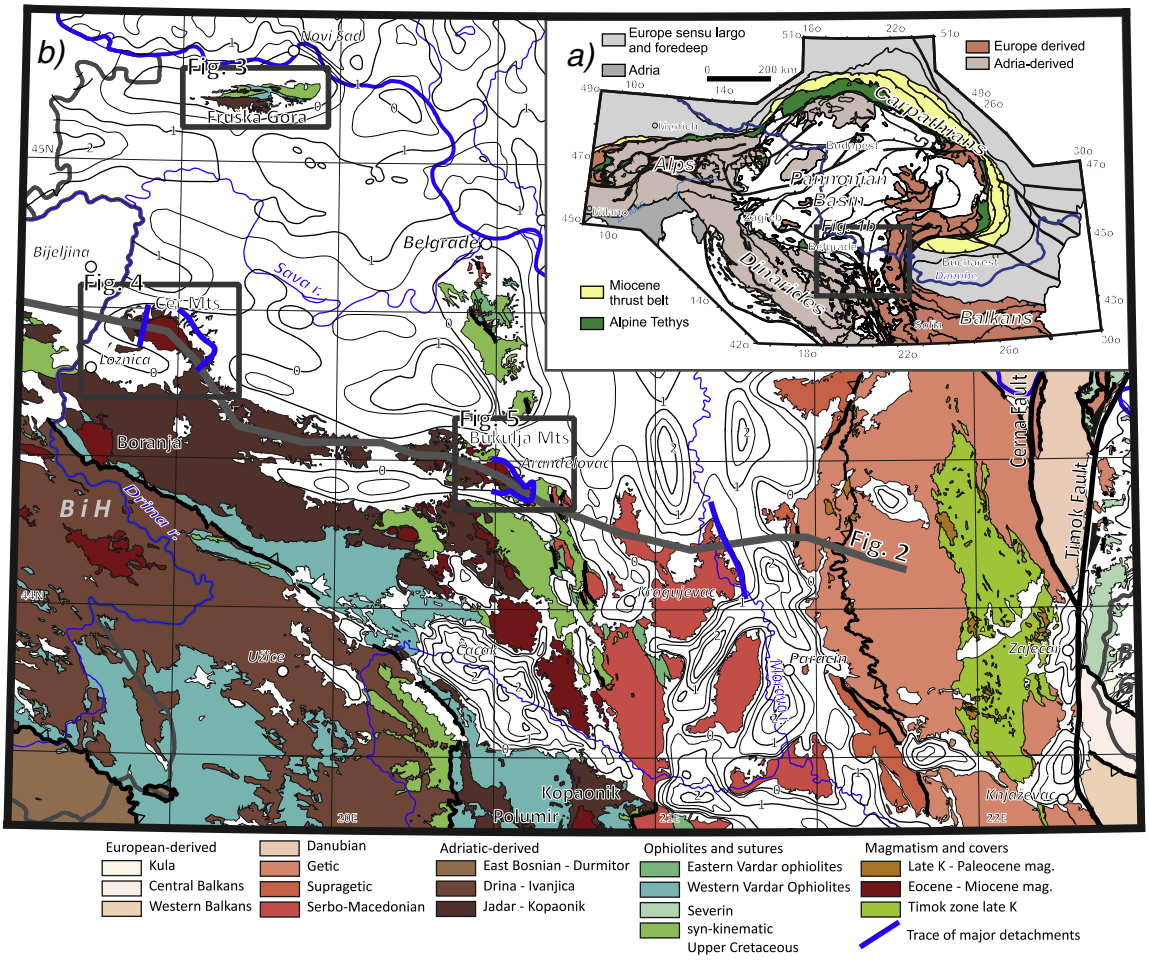

Fig. 1. a—Tectonic map of the Alps –Carpathians –Dinarides System (simplified after Schmid et al., 2008). The grey rectangle is the location of Fig. 1b. b—Detailed geological map of the connection between the Dinarides, South Carpathians and Pannonian Basin. The thick grey line is the locations of the cross-section in Fig. 2. The grey rectangles indicate locations of the maps in Figs. 3–5.

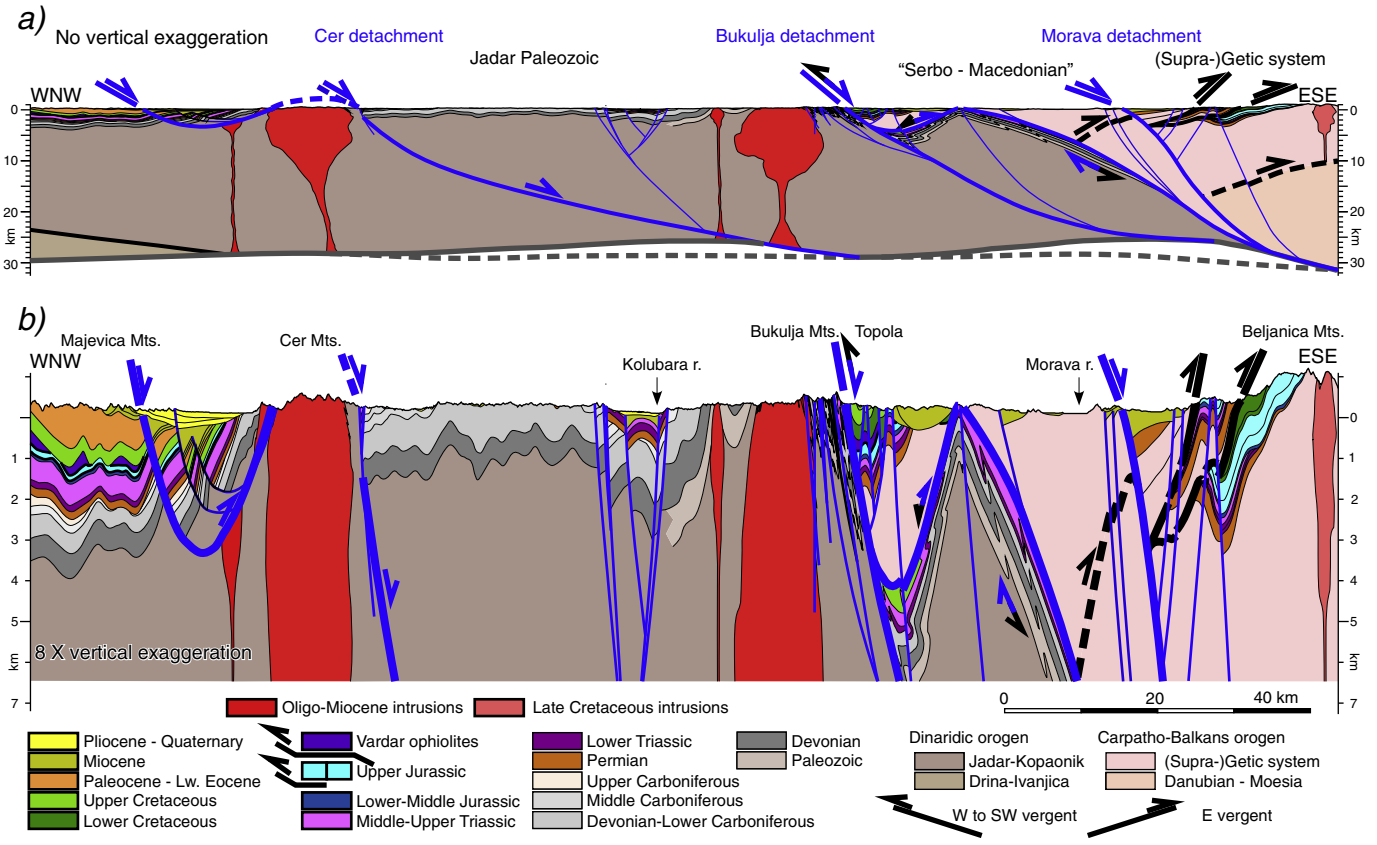

Fig. 2. a—Cross section across the NE Dinarides and Serbian part of the Carpatho-Balkanides b—The same cross section with 8× vertical exaggeration.

in the footwall of these detachments (Erak et al., in this issue; Stojadinovic et al., 2013; Toljić et al., 2013; Ustaszewski et al., 2010) combined with existing local or regional studies or synthesis (e.g., Dimitrijević, 1997; Toljić et al., submitted for publication).

2. The link between exhumation and basin evolution in the NE Dinarides

Middle Triassic continental rifting and associated magmatism followed by subsequent passive margin evolution created a SE European branch of the Neotethys Ocean that separated units of Adriatic and European continental affinities (e.g., Pamic, 1984; Schmid et al., 2008; Stampfli and Borel, 2002). Its subsequent closure by subduction culminated during late Jurassic–Earliest Cretaceous times with ophiolitic obduction, island-arc magmatism, and formation of genetically associated ophiolitic melanges over both the Adriatic and European margins. While a ~180 km long thrust sheet of ophiolites was emplaced over the Adriatic margin (Western Vardar Ophiolites), smaller ophiolites and island arc volcanics were also emplaced over the European margin (Eastern Vardar Ophiolites, Dimitrijević, 1997; Djeric and Gerzina, 2008; Djeric et al., 2007; Robertson et al., 2009; Schmid et al., 2008). The subsequent Cretaceous shortening led to the final consumption of the Neotethys Ocean that was associated with widespread calk-alkaline magmatism along a belt of calc-alkaline rocks colloquially referred to as "banatites". A long "banatitic" belt (Berza et al., 1998) at ~92–67 Ma was running in the European-derived hinterland along the strike from the Apuseni Mountains of Romania to the Carpatho-Balkanides units of Serbia and Bulgaria, and emplaced locally in extensional basins (e.g., Timok, Srednogorie, Cvetković et al., 2000, 2013; Gallhofer et al., 2015; von Quadt et al., 2005). The shortening culminated with the continental collision between Europe- and Adria- derived continental units in latest Cretaceous times, which created the Sava Suture Zone of the Dinarides (Pamić, 2002; Ustaszewski et al., 2009, 2010).

The overall contraction resulted in the formation of a fold and thrust belt. Within the thrust sheet architecture the three most internal ones (East Bosnian-Durmitor, Drina-Ivanjica, Jadar-Kopaonik) carry in an upper structural position Late Jurassic–earliest Cretaceous ophiolites (Figs. 1 and 2, e.g., Dimitrijević, 1997). The most internal unit that contains Triassic — Jurassic sediments of Adriatic affinity is the Jadar-Kopaonik composite unit (Schmid et al., 2008). These sediments crop out in the so-called Jadar block in the NW-most part of the studied segment of the Dinarides (Fig. 1, Dimitrijević, 1997; Karamata, 2006). This block is composed of a non- to slightly metamorphosed Paleozoic sequence covered by a Triassic–Jurassic shallow water carbonatic to deep water radiolaritic sequence, which is similar to various other tectonic slices observed in the Dinarides or neighboring Pannonian Basin (Filipović et al., 2003; Pamić, 2002; Tomljenovic et al., 2008). To the SE, this block is laterally continuous with the Kopaonik metamorphic series (Dimitrijević, 1997; Schmid et al., 2008) that are the metamorphosed equivalents of the Jadar Paleozoic and its Triassic — Jurassic sequence (Schefer, 2010; Schefer et al., 2010). East and north in the studied area in the hanging-wall of the Sava suture zone, Dacia is an European-derived block that consists of an *E*-vergent thick-skinned nappe stack (Danubian, Getic, Biharia and Supragetic nappes, including the Serbo-Macedonian "Massif", Fig. 1b). Adjacent to the study area, the Getic/Supragetic nappes and the Serbo-Macedonian Massif contain a medium to high-grade metamorphic Neoproterozoic to Early Paleozoic basement, locally overlain by low-grade Paleozoic successions and a sedimentary cover that contains Triassic–Lower Cretaceous dominantly continental to shallow-water carbonatic successions (e.g., Antić et al., 2016; Dimitrijević, 1997). Ophiolites obducted over both Europe-derived (Serbo-Macedonian) and Adriatic-derived (Jadar-Kopaonik) margins during late Jurassic–Earliest Cretaceous time were subsequently

juxtaposed by the Cretaceous–Eocene orogenic collision against the Sava suture zone (Fig. 1, Schmid et al., 2008).

In the northern part of the studied area, the Pannonian Basin (Fig. 1) is a continental back-arc basin that formed during the Miocene in response to the rapid roll-back of a sub-Carpathian slab attached to the European continent (Fig. 1, e.g., Horváth et al., 2015; Matenco et al., 2010). The extension is recorded in the Dinarides or at their northern margin along a large number of Late Oligocene–Miocene detachments reactivating the former suture zone or various nappe contacts in the Dinarides (e.g., Stojadinovic et al., 2013; Toljić et al., 2013; Ustaszewski et al., 2010). A latest Miocene–Quaternary contractional event has subsequently overprinted the NE margin of the Dinarides and the Pannonian Basin during the indentation of Adria (Bada et al., 2007; Fodor et al., 2005; Horváth, 1995; Pinter et al., 2005).

In the internal-most part of the Dinarides, distal deposits of Adriatic affinity were exhumed by the Miocene extension next to Upper Cretaceous–Paleogene sediments and are observed in the three main areas investigated by our study, i.e. Fruška Gora, Bukulja and Cer Mountains (Fig. 1b).

2.1. Evolution of the Adriatic margin and Cretaceous–Miocene sedimentation in the Fruška Gora Mountains

The Fruška Gora Mountains (Figs. 1b and 3) comprise a metamorphosed Paleozoic–Jurassic sequence and an overlying ophiolites of the Jadar-Kopaonik unit that are separated from their non-metamorphosed equivalents by a large scale extensional detachment system (Toljić et al., 2013; Stojadinovic et al., 2013). These rocks are overlain by an uppermost Cretaceous–Paleogene sedimentary sequence and rare Eocene volcanics (Fig. 3). Three successive contractional deformation events associated with burial, metamorphism, shearing and folding affected Fruška Gora during the latest Cretaceous–Paleogene contraction (Fig. 3b, Toljić et al., 2013), and were subsequently followed by a Late Oligocene–Miocene extension and formation of an extensional detachment (Toljić et al., 2013). The initial Late Oligocene–Early Miocene activity of the detachment was followed by Middle Miocene exhumation and normal faulting with ~19–11 Ma ZFT and AFT exhumation ages (Stojadinovic et al., 2013). The present large-scale open antiformal geometry of the Fruška Gora Mountains is an effect of the Pliocene–Quaternary tectonic inversion related to the Pannonian Basin.

Upper Cretaceous–Paleogene transgressive sediments (Figs. 3, 6a, b) start with coarse continental clastics, overlain by shallow water clastic and carbonate deposits that contain abundant Maastrichtian fauna (Čičulić and Rakić, 1977). These are overlain by a >2 km thick turbiditic sequence that contains Paleogene age microfauna in its upper parts (e.g., De Capoa et al., 2002; Fig. 6b). This thick succession of turbidites is generally interpreted as *syn*-contractional sediments (i.e. flysch) that were deposited during the latest Cretaceous collision (Dimitrijevic and Dimitrijevic, 1987; Schmid et al., 2008). The shallow

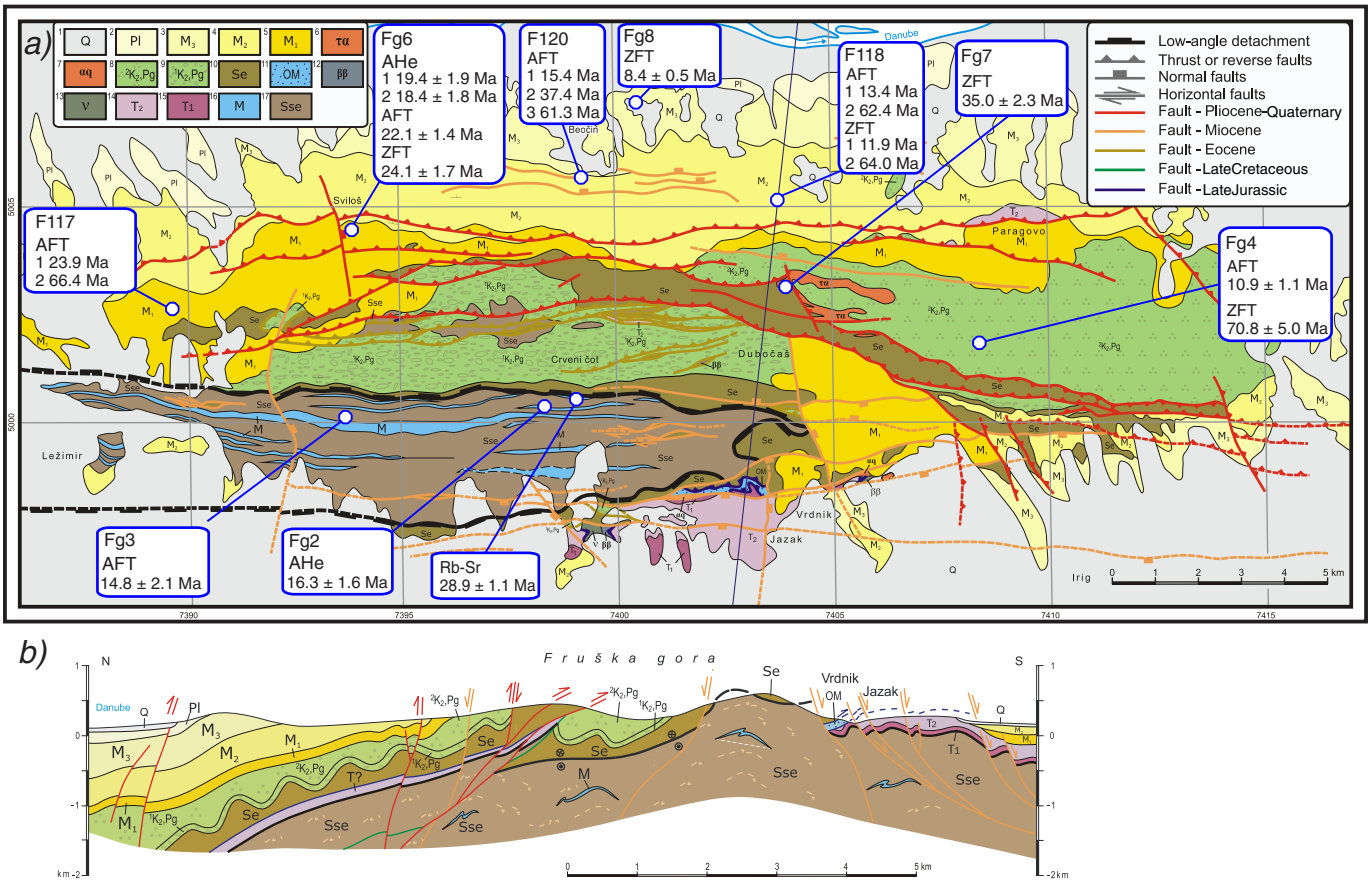

Fig. 3. a—Geological map of the Fruška Gora mountains, based on the Geological Map of Yugoslavia (1:100.000), sheet Novi Sad (Čičulić-Trifunović and Rakić, 1976), modified with observations and interpretations presented in study of Toljić et al. (2013), with low-t thermochronology ages obtained in the present study and study of Stojadinovic et al. (2013). AFT and ZFT ages are reported as central ages with ±1σ standard error in concordant samples, and best-fit peak ages in discordant samples. AHe ages are reported as single grain ages. Coordinates are in kilometers, system of projection MGI Balkan zone 7. Legend: 1—Quaternary; 2—Pliocene; 3—Upper Miocene; 4—Middle Miocene; 5—Lower Miocene; 6—Eocene–Oligocene latites; 7 —Eocene–Oligocene trachy-andesites; 8—Uppermost Cretaceous–Paleogene "Sava flysch"; 9—Upper Cretaceous–Paleogene; 10—Serpentinites; 11—Ophiolitic melange; 12—Diabase; 13 —Peridotite; 14—Middle Triassic; 15—Lower Triassic; 16—Marbles; 17—Sericite schists; b—NNE–SSW oriented geologic cross-sections over Fruška Gora along the direction of contractional shortening (legend and locations are presented in Fig. 3a).

water transgressive base strongly resembles the onset of deposition of the Gosau-style clastic-carbonatic sequence regionally observed in the Alps or the Carpathians (Schuller et al., 2009; Wagreich and Faupl, 1994; Willingshofer et al., 1999) although its age in the Fruška Gora Mountains is younger.

The Neogene sediments along the flanks of the Fruška Gora (Fig. 3a) were deposited unconformably over older deposits and start with Lower Miocene (Ottnangian–Karpatian) coarse continental clastics that pass rapidly into shallow-water lacustrine deposits (Fig. 7a). The latest Early Miocene–early Middle Miocene (Badenian) sedimentation starts with basal conglomerates and course-grained sandstones, intercalated with thick sequences of tuffs. These are overlain by early Middle Miocene shallow water carbonates and clastics. The thin late Middle Miocene (Sarmatian) sedimentation is laterally variable as an effect of the coeval extension and is observed as various clastics, from conglomerates to siltstones and clays (Fig. 7a). A gradually regressive stage of basin fill during Late Miocene (Pannonian) times was characterized by dominantly SE directed, laterally variable, prograding deposits (e.g., Magyar et al., 2013).

2.2. Evolution of the Adriatic margin and Cretaceous–Miocene sedimentation in the Cer and Bukulja Mountains

The Cer Mountains are an isolated topographic feature almost completely surrounded by Miocene–Quaternary sediments of the Pannonian basin in the NW part of the studied area (Figs. 1b and 4). The Cer intrusion, in the core of the mountains, is a composite pluton that comprises a predominantly I-type quartz-monzonite, which is subsequently intruded by a S-type two-mica granite, occurring as a large unit in the central-western part and meter-thick dykes in its eastern area (Fig. 4). A wide shear zone with widespread mylonitic foliation and stretching lineation is observed in the metamorphic rocks that separate the main Cer intrusion from an intrusion of granodiorites to quartz-monzonites that occurs at ~7 km towards the NW in the

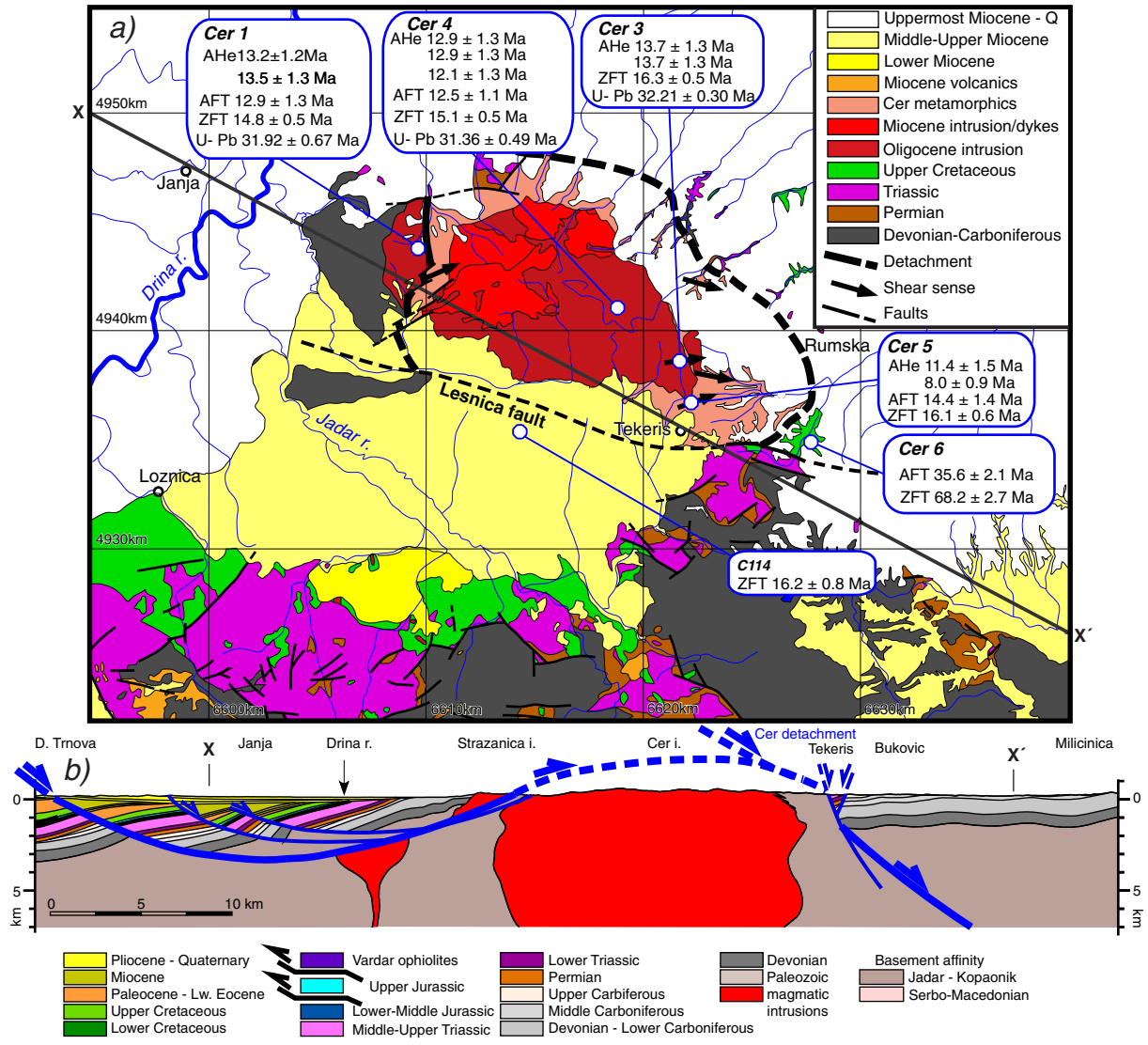

Fig. 4. a—Geological Map of the Cer Mountains based, on the Basic Geological Map of Yugoslavia (1:100.000) sheets Zvornik (Mojsilović et al., 1975) and Vladimirci (Filipović et al., 1971) with low-t thermochronology ages and high temperature U—Pb zircon ages obtained in the present study and study of Stojadinovic et al. (2013). AFT and ZFT ages are reported as central ages with ± 1σ standard error. AHe ages are reported as single grain ages. U—Pb zircon ages are reported as pooled crystallization ages. Numbers at the borders of the map are MGI Balkan 6 Cartesian coordinates; b—WNW–ESE oriented geologic cross-section across the Cer Mts along the direction of transport during extensional exhumation. The cross-section based on regional cross-section in Fig. 2. Marks XX′ label segment of the cross-section that cross-cuts map in Fig. 4a.

Stražanica area (Fig. 4, Cvetkovic et al., 2001; Koroneos et al., 2011). Whole-rock geochemistry supports a mixed origin of different types of magmas for these igneous rocks. I-type rocks were generated by a mantle source, emplaced at greater depths, and subsequently affected by the S-type rocks derived by crustal melts emplaced at shallow depths. Previous K—Ar absolute ages measured in all types of Cer intrusions indicate scattered and non-homogenous ages spanning between 21 and 15 Ma (Koroneos et al., 2011). The country rocks are part of the Jadar-Kopaonik unit, composed here of Paleozoic siliciclastic sediments with carbonatic intercalations, slightly metamorphosed to sub-greenschists facies, and covered by a Permian–Triassic mostly carbonatic succession that are tectonically overlain by Western Vardar ophiolitic melange and ophiolites (Krstić et al., 2005; Robertson et al., 2009). The southern flank of the Cer Mountains is affected by a large E-W oriented Miocene normal fault (the Lešnica Fault, Fig. 4).

The Cer Mountains Paleozoic–Jurassic sequence is unconformably overlain by a thin late Cretaceous cover section, which starts with Turonian conglomerates and shallow water limestones that gradually passes upwards to Campanian–Maastrichtian clastics, shallow water limestones and turbidites (Mojsilović et al., 1975). These rocks are unconformably covered almost on all sides of the Cer Mountains by Miocene–Quaternary sediments (Figs. 4, 7c) that start with Middle Miocene coarse continental conglomerates and shallow water sandstones gradually deepening to laterally variable Upper Miocene clastics.

The Bukulja Mountains (Fig. 5) are cored by an S-type leucocratic pluton consisting dominantly of a two-mica granite with 20–15 Ma K—Ar ages (Cvetković et al., 2007). This intrusion is interpreted to have been derived from magmas generated by intensive crustal thinning associated with the extension of the Pannonian basin (Cvetković et al., 2007). The western flank of the pluton is intruded into the Paleozoic series of the Jadar block made up of clastics alternating with basic volcanics and volcanoclastics metamorphosed in greenschist facies, or retromorphosed from an initial higher amphibolite facies (the Drina Formation of Karamata et al., 2003; Trivić et al., 2010). Interpreted as

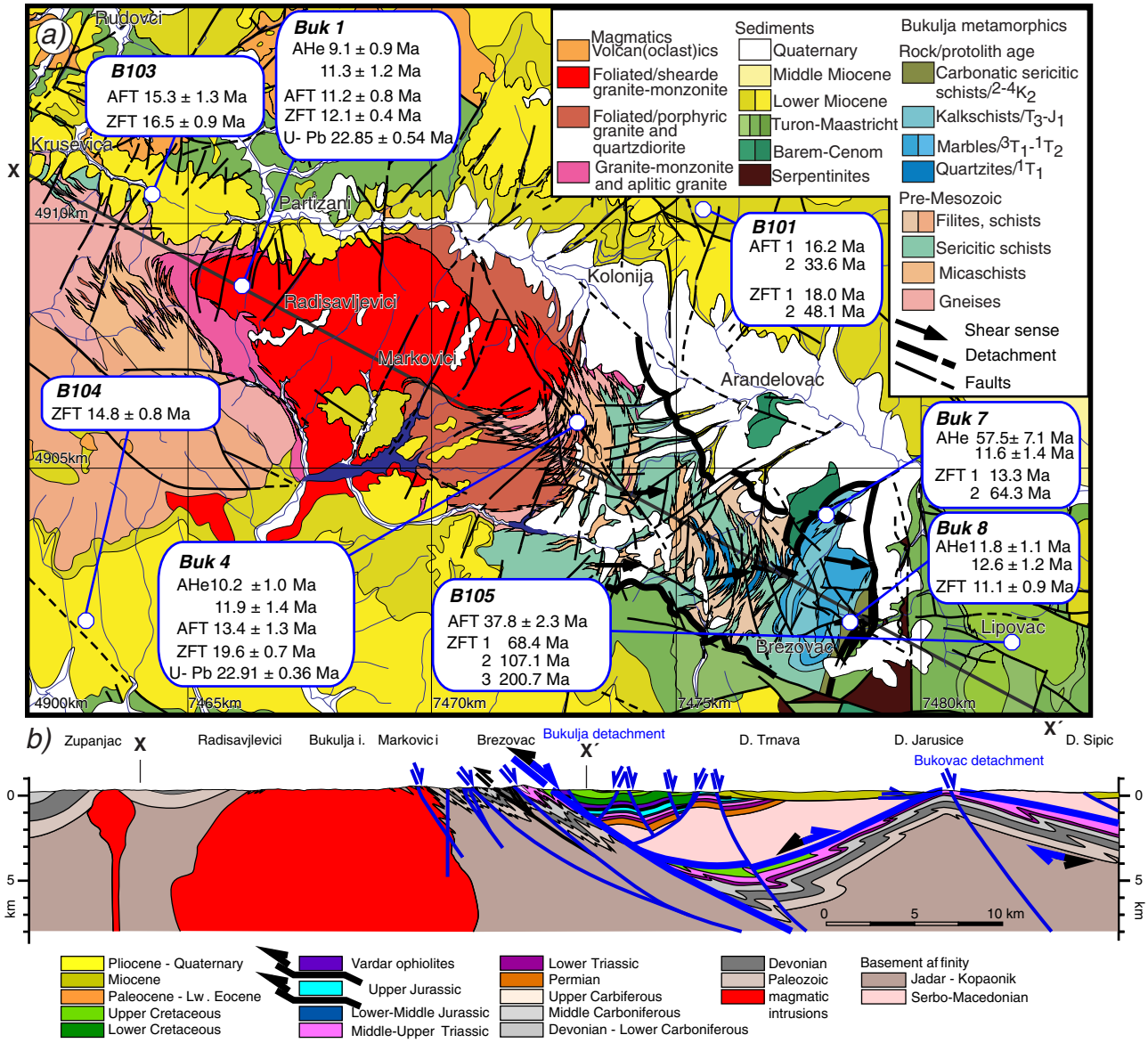

Fig. 5. a—Geological Map of the Bukulja Mountains, based on the Basic Geological Map of Yugoslavia (1:100.000) sheets Obrenovac (Filipović et al., 1979), Smederevo (Pavlović et al., 1979), Gornji Milanovac (Filipović et al., 1976) and Kragujevac (Brković et al., 1979) with low-t thermochronology ages and high temperature U—Pb zircon ages obtained in the present study and study of Stojadinovic et al. (2013). AFT and ZFT ages are reported as central ages with ±1σ standard error in concordant samples, and best-fit peak ages in discordant samples. AHe ages are reported as single grain ages. U—Pb zircon ages are reported as pooled crystallization ages. Numbers at the borders of the map are MGI Balkan 7 Cartesian coordinates. b—WNW–ESE oriented geologic cross-section across the Bukulja Mts along the direction of transport during extensional exhumation. The cross-section based on regional cross-section in Fig. 2. Marks XX′ label segment of the cross-section that cross-cuts map in Fig. 5a.

contact metamorphism generated by the Miocene pluton, this facies decreases farther westwards to the usual greenschist to sub-greenschist facies of the Jadar block (Filipović et al., 2003; Marović et al., 2007). The eastern flank of the pluton is intruded into a sequence composed of various types of metamorphics (Fig. 5, see also Stojadinovic et al., 2013). The lower parts of these metamorphic rocks locally contain Paleozoic fauna (the lower part of the Birač Formation of Trivić et al., 2010) while an Upper Cretaceous protolith has been interpreted in its upper parts (in the upper part of the Bukulja-Venčac crystalline of Marović et al., 2007). The intermediate sequence is interpreted as a Triassic–Jurassic sequence of the Jadar unit metamorphosed in greenschist facies conditions and exhumed by a large scale detachment (Stojadinovic et al., 2013). Hence, the position of detachment reflects specific extensional geometry of the Bukulja Mts half-dome. The northern, eastern, and southern flank of its magmatic/metamorphic core show strong structural and lithostratigraphic contrast along major shear zone with the surrounding non-metamorphosed units. At the same time the western flank of Bukulja doesn't show any tectonic omission (Figs. 2 and 5). In the hanging-wall of this detachment, Late Cretaceous turbidites of the Sava zone crop out together with a Cretaceous–Paleogene sequence that unconformably overlies the ophiolites and the ophiolitic melange of the East Vardar Unit thrusted over the Serbo-Macedonian unit during Late Jurassic times (Fig. 5, Schmid et al., 2008).

Two sedimentary cycles are observed in the Cretaceous-Paleogene deposits flanking the Bukulja Mountains to the east (Fig. 6c). The Lower Cretaceous starts with unconformable continental conglomerates that gradually give way to a shallow water sequence that is laterally and upwards variable. In more proximal areas shallow water reef limestones (typical Urgonian facies) are overlain or laterally replaced by Lower Cretaceous clastic shelf deposits varying from massive sandstones to cyclic sandstones - siltstones alternations (the "para-flysch" of Dimitrijević, 1997). Near the structural contact with the metamorphosed succession of the Bukulja Mountains, these rocks are unconformably covered by a second Turonian–Maastrichtian (possibly also Paleocene, see Marović et al., 2007) cycle (Fig. 6c). This facies partly displays the turbiditic features that are typical for the Maastrichtian sediments of the Sava zone.

The onset of Lower Miocene sedimentation on the flanks of the Bukulja Mountains (Fig. 5) is characterized by the same alluvial, lacustrine to marine sequence as observed in the Fruška Gora Mountains. However, on the flanks of the Bukulja Mountains these are less well dated and are grouped together in a Lower–Middle Miocene sequence (e.g., Marović et al., 2007). This sedimentation started with basal conglomerates, followed by sandstones and clays, with intercalated volcaniclastics. Middle to Late Miocene sedimentation is represented by coarse clastic conglomerates, followed by finer-grained clastics and carbonates (Fig. 7b).

3. Detrital thermochronology of the NE Dinarides

Detrital thermochronology can unravel the important features of a source-sink system, considering broader context of the long-term evolution of an orogen. Combined zircon and apatite fission-track dating of the same sediment sample provides good balance between the number

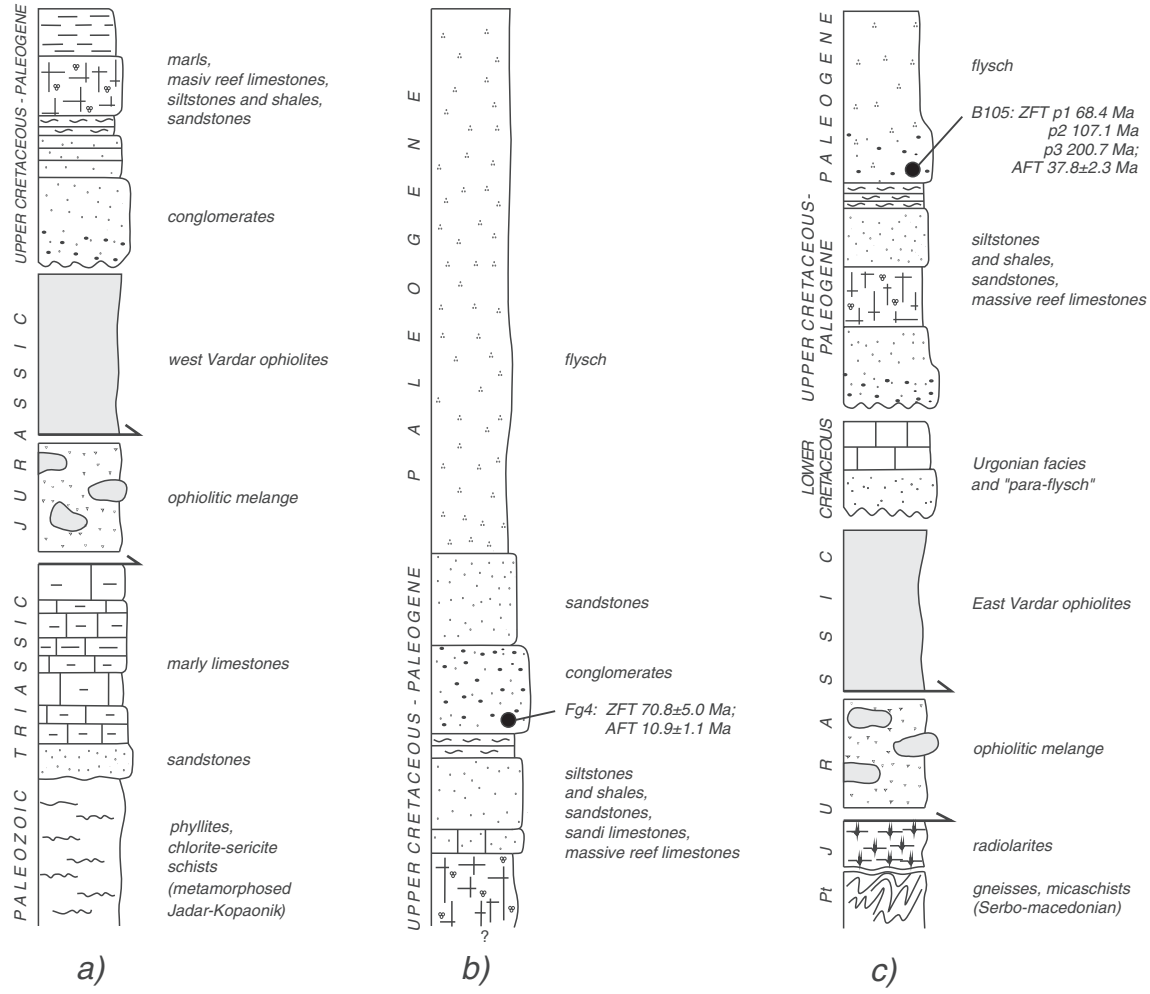

Fig. 6. Stratigraphic columns of Mesozoic to Paleogene sedimentary sequences of the Fruška Gora (a, b) and Bukulja Mountains (c), with positions of analyzed fission track samples.

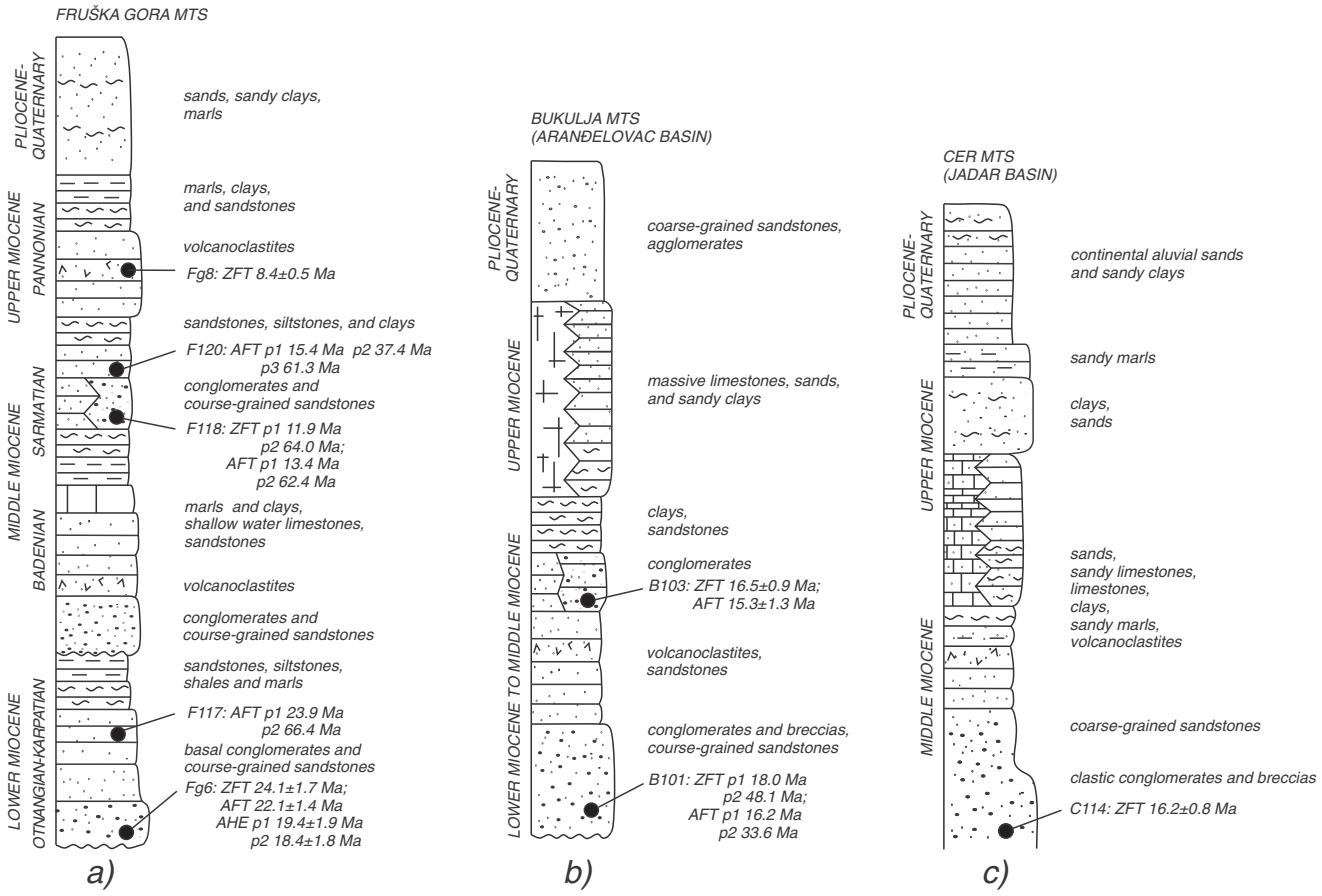

Fig. 7. Stratigraphic columns of Miocene sedimentary sequences of the Fruška Gora (a), Aranđelovac Basin (b), and Jadar Basin (c), with positions of analyzed fission track samples.

of grain age populations and the precision of the obtained ages (Garver et al., 1999; Spiegel et al., 2004). Furthermore, this combined approach reveals sediment provenance and, potentially, allows for the reconstruction of thermal history and exhumation of sediment source areas. More specifically, this may include identifying potential sources of the sediments, constrains on the time, rates and amounts of exhumation of the source areas, and new inferences on the main driving mechanisms of the erosion-transport-accumulation system. When applying single grain detrital zircon fission-track analysis in provenance and exhumation studies, the younger age component within conglomerates deserves special attention. Isolation of the youngest single grain age component allows the determination of the maximum age of sediments deposition. In the case of *syn*-kinematic conglomerates this will, furthermore, provide information on timing and rates, perhaps even the style and type, of exhumation processes active in the hinterland sourcing these conglomerates. In addition, thus obtained zircon fission track ages coupled with apatite fission track dating and thermal modelling of the same samples enable the reconstruction of their complete thermal histories, including the period from the moment of their deposition onwards.

We used detrital thermochronology to determine the evolution of Cretaceous–Paleogene and Miocene sediments in the areas of Bukulja, Cer, and Fruška Gora Mountains (Figs. 3–7). The results obtained in the present detrital thermochronology study are summarized in Tables 1 and 2, the detailed analytical procedures are presented in Appendix A, while sample locations are presented in Figs. 3–5.

3.1. Detrital thermochronology of Late Cretaceous–Paleogene sediments

Zircon and apatite fission track measurements were performed on three medium to very coarse grained conglomerates intercalated in the Late Cretaceous–Paleogene turbiditic succession in all three main analyzed areas (samples B105, Cer6, Fg4; Figs. 3–6). Two out of three zircon samples (Cer6 and Fg4) passed the Chi-square (χ^2). Sample B105 had P (χ^2) value of <5%, which indicates the presence of more than one age component (Table 1) and therefore a decomposition of this sample was conducted (Fig. 8c). All three apatite turbiditic conglomerate samples have passed the Chi-square (χ^2) test (Table 2). Mean track lengths range between 13.02 ± 1.24 and 14.22 ± 0.76 μm. Average D_{par} values are between 1.4 ± 0.2 and 1.7 ± 0.2 μm (Table 2).

Sample B105 is located on the south-eastern flank of the Bukulja Mountains (Figs. 2a, 5a, and 6c). Zircon fission track age measurements yielded a ZFT mean age of 89.5 ± 6.6 Ma that failed Chi-square (χ^2) test (Table 1). Statistical decomposition of the sample using BinomFit indicates three best-fit peak ages of 200.7 Ma, 107.1 Ma, and 68.4 Ma (Fig. 8c). The two older, subordinate age components of 200.7 Ma and 107.1 Ma, consist of zircon grains with rounded morphologies that may indicate potential metamorphic or reworked sediment sources and relatively longer sedimentary transport. The youngest and dominant population of provenance ages of 68.4 Ma, is composed of euhedral zircon grains, and it indicates a potential magmatic source that cooled during Maastrichtian times. In addition, the χ^2 age method was implemented to calculate the youngest age component within the sample. The pooled zircon fission track age is 68.2 ± 3.7 Ma, which is in agreement with the youngest best-fit peak age and, in this case, reveals the oldest age of deposition (Fig. 8c). Apatite fission track age measurement on the same sample provides a Late Eocene AFT central age of 37.8 ± 2.3 Ma, which is significantly younger than the obtained ZFT ages. The mean track length has a value of 13.02 ± 1.24 μm (54 track measured), while the average D_{par} is 1.5 ± 0.2 μm (Table 2). Existing stratigraphic observations and microfaunal evidences (Marović et al., 2007) indicate

Table 1
Zircon Fission Track (ZFT) Data. Bold numbers represent central ages with 1σ standard error in concordant ZFT samples, and best-fit peak ages in discordant ZFT samples. Central ages are calculated using dosimeter glass CN1, with zeta factor of 134 ± 5. Concordant samples are distinguished by having only one reported age. Abbreviations: No. grains—number of dated zircon crystals; Ns (Ni)—number of spontaneous (induced) tracks counted; ρs (ρi)—spontaneous (induced) track densities; Nd—number of tracks counted on the dosimeter; ρd—dosimeter track density; P (χ^2)—probability obtaining Chi-square (χ^2) for n degrees of freedom (n is number of crystals); Disp.—dispersion in single grain ages; Pop.—age populations calculated using BINOMFIT; Ab.(%)—abundance of the age component in the total single grain age distribution of a sample.

Sample code	Location	Rock type	Stratigraphic age	Age (±1σ) (Ma)	No. grains	Ns ($\times 10^6$ cm^{-2})	ρs	Ni ($\times 10^6$ cm^{-2})	ρi	Nd ($\times 10^6$ cm^{-2})	ρd (%)	P (χ^2)	Disp.	Pop. morph.	Grain (Ma)	Age (%)	Ab.
Fg4	Fruška Gora	Turbiditic conglomerates	Maastrichtian	**70.8 ± 5.0**	22	880	3512	450	1,96	8875	0.543	100.00	0.00		Euhedral		
Cer6	Cer	Turbiditic conglomerates	Maastrichtian	**68.2 ± 2.7**	20	2742	8982	1251	4098	8875	0.543	98.76	0.00		Euhedral		
B105	Bukulja	Turbiditic conglomerates	Maastrichtian	89.5 ± 6.6	29	4317	7384	1832	3134	8875	0.543	0.00	0.23	1	Euhedral	**68.4**	60.9
														2	Rounded	**107.1**	33.8
														3	Rounded	**200.7**	5.3
Fg6	Fruška Gora	Conglomerates	Upper Lower Miocene	**24.1 ± 1.7**	19	514	3095	776	4672	8875	0.543	99.61	0.00		Rounded		
F118	Fruška Gora	Conglomerates	Upper Middle Miocene	36.5 ± 5.6	23	1410	3875	1593	4378	8875	0.543	0.00	0.79	1	Rounded	**11.9**	52.2
														2	Euhedral	**64.0**	47.8
Fg8	Fruška Gora	Tuffs	Upper Miocene	**8.4 ± 0.5**	24	476	1535	2057	6634	8875	0.543	99.95	0.00		Euhedral		
B101	Bukulja	Conglomerates	Lower to Middle Miocene	22.7 ± 2.6	20	520	1617	901	2802	8875	0.543	0.04	0.29	1	Rounded	**18.0**	85.1
														2	Rounded	**48.1**	14.9
B103	Bukulja	Conglomerates	Middle Miocene	**16.5 ± 0.9**	28	890	2092	1957	4602	8875	0.543	99.57	0.00		Euhedral		
B104	Bukulja	Conglomerates	Middle Miocene	**14.8 ± 0.8**	27	848	2381	2089	5865	8875	0.543	99.30	0.00		Euhedral		
C114	Cer	Conglomerates	Middle Miocene	**16.2 ± 0.8**	41	1882	4081	4320	9171	8875	0.543	99.09	0.00		Euhedral		

that the deposition of these sediments occurred during the end of Cretaceous to early Paleogene times. Therefore, this AFT age represents the result of post-depositional burial followed by Late Eocene exhumation. The positively skewed horizontal confined track length distribution (Fig. 8c) typically occurs in apatite samples which have experienced prolonged heating followed by the rapid cooling from the upper limit of apatite PAZ (Carter and Gallager, 2004). Pooled zircon fission track age of 68.2 ± 3.7 Ma of the youngest age population, was used as additional constraint in thermal modelling of sample B105, setting the oldest time of its deposition to Maastrichtian. The results of modelling allow for the possibility of a late Eocene cooling event, taking place after progressive heating by burial to temperatures close to the upper limit of the apatite PAZ (~120 °C) during the Paleocene –Eocene period (Fig. 8c). The burial was deep enough to reset the AFT, but not deep enough to reset the ZFT.

Similar results were obtained for the turbiditic sample Cer6 from the eastern flank of the Cer Mountains (Fig. 4a). The ZFT central age is 68.2 ± 2.7 Ma, which is a provenance age that reflects Maastrichtian cooling of a sediment source area (Fig. 8b). Euhedral morphologies of zircon grains indicate existence of potential magmatic source(s). Measured apatite fission track central age of the same sample is 35.6 ± 2.1 Ma, with a mean track length of 14.22 ± 0.76 μm (50 tracks measured, Table 2). This is an exhumation age, indicating subsequent burial and Late Eocene cooling through the partial annealing zone of apatite (Fig. 8b). Thermal modelling of sample Cer6 demonstrates its rapid cooling from the upper limit of the zircon partial annealing zone (ZPAZ, ~200 °C) to the superficial depositional temperatures which occurred in the latest Cretaceous (Maastrichtian) to Paleocene time. After heating due to burial, the sample has experienced rapid Late Eocene cooling through the partial annealing zone of apatite (APAZ, Fig. 8b). The burial was deep enough to reset the AFT, but not deep enough to reset the ZFT. After the Late Eocene, a significantly lower cooling rate below the APAZ is inferred (Fig. 8b).

Sample Fg4 was collected from the Maastrichtian–Paleocene turbidites exposed in the NE part of Fruška Gora (Figs. 1b, 3a, and 6b). Given the position in the stratigraphic sequence, the ZFT central age of 70.8 ± 5.0 Ma with homogeneous single-grain ages distribution represents a provenance age that reflects Latest Cretaceous cooling of the source area (Fig. 8a). The homogeneous population is comprised of zircon grains with euhedral morphologies, indicating potential magmatic source(s) and relatively short transport/fast deposition of the sediments. Apatite fission track age measurements on the same sample yielded an AFT central age of 10.9 ± 1.1 Ma (Fig. 8a). Horizontal confined track length measurements give mean track length of 13.95 ± 0.86 μm (82 tracks measured), while the average value of the D_{par} is 1.7 ± 0.2 μm (Table 2). High value of the mean track lengths and narrow length distributions are indicators of post - Cretaceous burial and heating above ~120 °C, followed by rapid post-depositional cooling of the sample through the partial annealing zone of apatite (APAZ, ~140–100 °C) that occurred in the early Late Miocene, as inferred by the result of the thermal modelling (Fig. 8a). The burial was deep enough to reset the AFT, but not deep enough to reset the ZFT. A rapid late Middle–early Late Miocene (between 14 and 10 Ma) cooling event through the partial annealing zone of apatite (APAZ, Fig. 8a) brought the sample close to the surface.

3.2. Detrital thermochronology of Miocene sediments in the Fruška Gora Mountains

Two out of the three Fruška Gora Miocene samples used in ZFT analyses passed the Chi-square (χ^2) test (samples Fg6 and Fg8, Fig. 3a, Table 1). Sample F118 had P (χ^2) value of <5%, therefore decomposition of this sample was performed with the BinomFit software (Fig. 9c). Only one out of four apatite samples from the Fruška Gora Miocene sequence passed the Chi-square (χ^2) test (sample Fg6, 3a, Table 2). The remaining three samples did not pass the Chi-square (χ^2) test and were

Table 2
Apatite Fission Track (AFT) Data. Bold numbers represent central ages with 1σ standard error in concordant AFT samples, and best-fit peak ages in discordant AFT samples. Central ages are calculated using dosimeter glass CN5, with zeta factor of 349 ± 15. Concordant samples are distinguished by having only one reported age. Abbreviations: No. grains—number of dated apatite crystals; Ns (Ni)—number of spontaneous (induced) tracks counted; ρs (ρi)—spontaneous (induced) track densities; Nd—number of tracks counted on the dosimeter; ρd—dosimeter track density; P (χ^2)—probability obtaining Chi-square (χ^2) for n degrees of freedom (n is number of crystals); Disp.—dispersion in single grain ages; Pop.—age populations calculated using BINOMFIT; Ab.(%)—abundance of the age component in the total single grain age distribution of a sample; MTL—c-axis projected mean track length with standard deviation (SDl) in track length distribution; Nl—number of measured confined tracks; D_{par}—average etch pit diameter with its standard deviation.

				Age Data													Length data		
Sample code	Location	Rock type	Stratigraphic age	Age (±1σ) (Ma)	No. grains	Ns ($\times 10^6$ cm^{-2})	ρs ($\times 10^6$ cm^{-2})	Ni	ρi ($\times 10^6$ cm^{-2})	Nd (%)	ρd	P (χ^2)	Disp. (Ma)	Pop. (%)	Age	Ab. (μm)	MTL ± SDL (μm)	NL	Dpar ± SDDpar
Fg4	Fruška Gora	Turbiditic conglomerates	Maastrichtian	**10.9 ± 1.1**	15	200	0.202	2517	2541	8040	1204	93.05	0.00				13.95 ± 0.86	82	1.7 ± 0.2
Cer6	Cer	Turbiditic conglomerates	Maastrichtian	**35.6 ± 2.1**	25	683	0.493	4023	2906	8040	1204	99.76	0.00				14.22 ± 0.76	50	1.4 ± 0.2
B105	Bukulja	Turbiditic conglomerates	Maastrichtian	**37.8 ± 2.3**	29	687	0.604	3807	3346	8040	1204	100.00	0.00				13.02 ± 1.24	54	1.5 ± 0.2
Fg6	Fruška Gora	Conglomerates	Upper Lower Miocene	**22.1 ± 1.4**	27	509	0.251	4829	2385	8040	1204	99.90	0.00				14.11 ± 0.74	12	1.4 ± 0.2
F117	Fruška Gora	Sandstones	Upper Lower Miocene	51.6 ± 2.8	61	1054	0.368	4255	1484	8040	1204	0.00	0.34	1	**23.9**	33.5	13.81 ± 0.53	5	1.3 ± 0.2
														2	**66.4**	66.5	13.32 ± 0.50	10	1.6 ± 0.4
F118	Fruška Gora	Conglomerates	Upper Middle Miocene	36.1 ± 4.2	38	751	0.259	5184	1786	8040	1204	0.00	0.70	1	**13.4**	55.3	13.98 ± 1.01	17	1.8 ± 0.3
														2	**62.4**	44.7	13.62 ± 1.13	16	1.9 ± 0.4
F120	Fruška Gora	Sandstones	Upper Middle Miocene	28.9 ± 2.9	40	383	0.187	3102	1514	8040	1204	0.00	0.52	1	**15.4**	57.2	14.06 ± 0.80	12	1.5 ± 0.2
														2	**37.4**	28.4	14.38 ± 0.76	7	1.8 ± 0.2
														3	**61.3**	14.4			1.7 ± 0.2
B101	Bukulja	Conglomerates	Lower to Middle Miocene	25.5 ± 2.1	27	248	0.138	2319	1288	8040	1204	0.92	0.28	1	**16.2**	53.0	14.64 ± 0.54	7	1.3 ± 0.3
														2	**33.6**	47.0	13.22 ± 1.16	18	1.6 ± 0.3
B103	Bukulja	Conglomerates	Middle Miocene	**15.3 ± 1.3**	26	214	0.119	2938	1631	8040	1204	100.00	0.00				14.14 ± 1.13	25	1.3 ± 0.2

decomposed using the BinomFit software (Fig. 9). When apatite detrital samples showed homogeneous distribution of single grain ages and there was no evidence of significant post-depositional thermal overprint (i.e. AFT ages older than stratigraphic ages), the measured horizontal confined tracks were considered in interpretation (samples Fg4 and Fg6, Table 2). In this case the tracks reflect the thermal history of their source area.

Sample Fg6 was taken from the Lower Miocene basal coarse clastics deposited along the NW flank of the Fruška Gora (Figs. 3a; 7a). ZFT measurements yielded a central age of 24.1 ± 1.7 Ma, indicating a homogeneous age distribution (Fig. 9a). Zircon grains expose rounded morphologies as an indication of re-working in the source area. AFT measurements in the same sample resulted in a central age of 22.1 ± 1.4 Ma with a homogeneous distribution (Fig. 9a). AFT confined track lengths are 14.11 ± 0.74 μm with the average value of the D_{par} of 1.4 ± 0.2 μm (Table 2). Previously reported AHe single grain ages of 19.4 ± 1.9 Ma and 18.4 ± 1.8 Ma obtained in this sample reflect cooling at superficial crustal levels (Fig. 3a, Stojadinovic et al., 2013). Overall, these measurements indicate a fast cooling event in the source area between ~24–18 Ma. The stratigraphic age of the sample is overlapping within its error bars the AHe cooling ages, meaning very fast exhumation and re-deposition after the AHe age.

Sample F117 was taken from a Lower Miocene coarse intercalation in an upper stratigraphic interval in the vicinity of the previously described sample (Figs. 3a and 7a). An AFT mean age of 51.6 ± 2.8 Ma has been obtained with the χ^2 probability value indicative for mixed age distribution (Table 2). Statistical decomposition of age distributions indicates two best-fit peak ages of 23.9 Ma and 66.4 Ma (Fig. 9d). The younger age of ~24 Ma is older than the Lower Miocene stratigraphic age of these sediments and indicate a similar source area with the previously described sample Fg6 (Figs. 7a and 9). The older age component of ~66 Ma shows an influx of material of a different source rock that exhumed in Maastrichtian times and can be a re-worked sediment source.

Sample F118 was collected in an upper stratigraphic interval, in a coarse intercalation of the late Middle Miocene (Sarmatian) marine clastics along the northern flank of Fruška Gora (Figs. 3a, 7a). ZFT provided a mean age of 36.5 ± 5.6 Ma, which did not pass the χ^2 test. Decomposition revealed two best-fit peak ZFT ages of 11.9 Ma and 64 Ma; both components consisting of grains with rounded morphologies (Fig. 9c). The mean AFT age of this sample is 36.1 ± 4.2 Ma and the failed χ^2 test. Statistical decomposition indicates two best-fit peak AFT ages of 13.4 Ma and 62.4 Ma (Fig. 9c). It is difficult to believe that a ZFT age population is older than the corresponding AFT, therefore these results have to be considered within their error bars (Tables 1, 2, Figs. 3 and 9c). On the overall, these results suggest fast cooling and exhumation in the source areas at two time intervals, ~62–64 Ma and 13–11 Ma. Given the fact the stratigraphic age of the sample is around 11–10 Ma, this also indicates its rapid exhumation and re-sedimentation during late Middle Miocene times.

Sample F120 has a similar late Middle Miocene age as the previous one, but is located in a slightly higher stratigraphic interval. Having failed the χ^2 test, statistical decomposition of AFT age distributions, reveal three best fit peak ages (Fig. 9e). The two older age components cluster at 61.3 Ma and 37.4 Ma, whereas the youngest age component clusters at 15.4 Ma (Table 2). In all cases the provenance ages reflect the exhumation of one or multiple source areas.

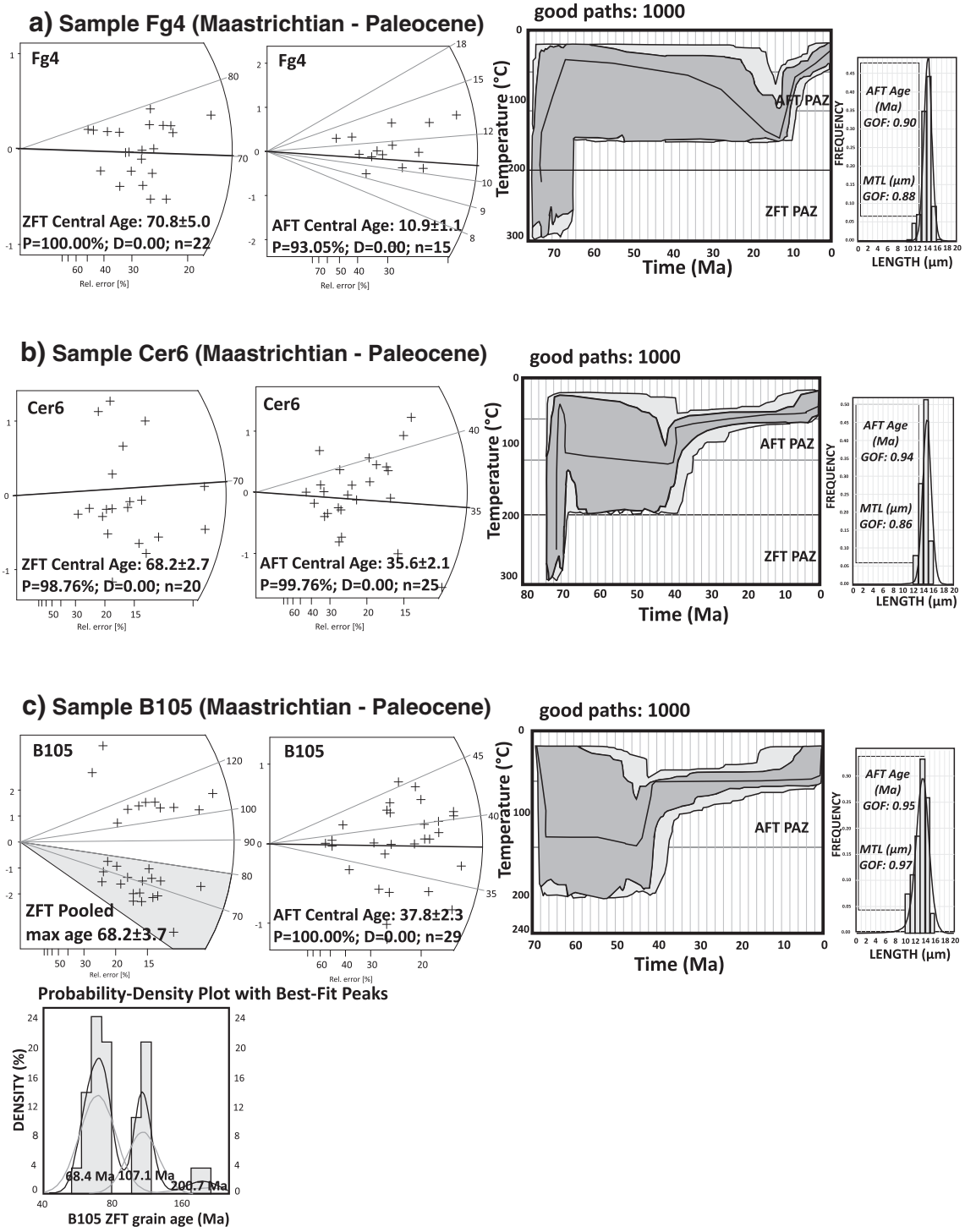

Fig. 8. Detrital thermochronology of three turbiditic flysch samples from the Fruška Gora (8a, sample Fg4), Cer (8b, sample Cer6), and Bukulja Mountains (8c, sample B105). The radial plots on the left that represent ZFT and AFT single grain age distributions were obtained using the TrackKey software (Dunkl, 2002). Central ages of the samples are indicated by solid black lines, and the youngest age populations for heterogeneous samples are indicated by grey shaded areas. Abbreviations: n- number of grains counted; Ages are central ages or pooled ages of youngest population; P—probability obtaining Chi-square (χ^2); D—dispersion in single grain ages. Probability-Density Plots with Best-Fit Peaks for heterogeneous samples were obtained using the BinomFit software (Brandon, 2002). Graphs on the right represent results of thermal modelling of AFT data of three flysch samples. Modelling was performed using HeFty program (Ketcham et al., 2003). AFT age data, track length distributions, and etch pit diameters (D_{par}) were used as input parameters. ZFT central ages were used to construct additional user-defined time-temperature boxes. The modeled t-T paths are extended into the zircon partial annealing zone (ZPAZ, solid black lines) between 300 and 200 °C (Brandon et al., 1998; Tagami, 2005). Partial annealing zone for apatite (APAZ) between 120 and 60 °C was confined by the solid dark grey lines (Laslett et al., 1987). The inverse Monte Carlo algorithm with annealing model of Ketcham et al. (1999, 2009) was used for generating the time-temperature paths. The light grey envelopes represent 'acceptable', and the dark ones 'good' fits between modeled and measured data.

Sample Fg8 is taken from a volcaniclastic material located in the lower part of the late Miocene (Pannonian) sequence (Figs. 3a and 7a). Its ZFT central age is of 8.4 ± 0.5 and indicates homogeneous distribution of single grain ages (Fig. 9b). The ZFT age is within the error bars of the stratigraphic age of this sample. In this particular case it is rather clear that the age reflects magmatic cooling during the

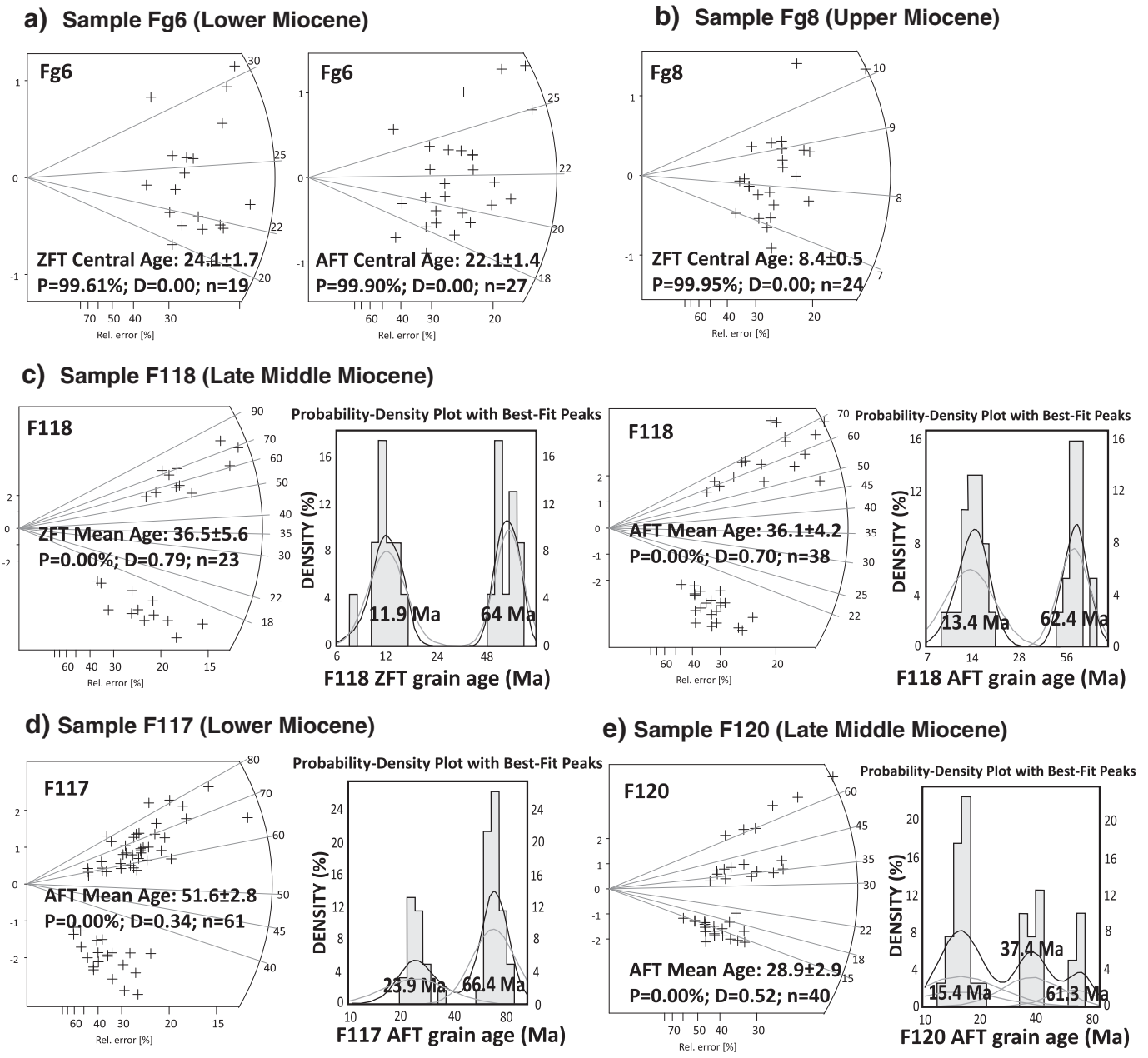

Fig. 9. ZFT and AFT detrital thermochronology of samples from the Fruška Gora Mountains. The radial plots representing ZFT and AFT single grain age distributions were obtained using the TrackKey software (Dunkl, 2002). Probability-Density Plots with Best-Fit Peaks for heterogeneous samples were obtained using the BinomFit software (Brandon, 2002). Abbreviations: n-number of grains counted; Ages are central ages or unweighted mean ages; P—probability obtaining Chi-square (χ^2); D—dispersion in single grain ages.

emplacement of the volcaniclastic material. Therefore, the ZFT age dates the age of the volcanic event responsible for the regional distribution of these tuffs. This is in agreement with similar ages of volcanic or volcaniclastic emplacement observed elsewhere in the intra-Carpathian region (Pécskay et al., 2006; Seghedi and Downes, 2011), but this is novel information in the studied area of northern Serbia. It is important for the absolute age correlation of the otherwise poorly dated Pannonian sediments.

3.3. Detrital thermochronology of Miocene sediments in the Bukulja and Cer Mountains

Zircon fission track measurements were conducted on 4 coarse samples, in the Miocene sediments located adjacent to Cer and Bukulja Mountains (Figs. 1b, 4, and 5).

Sample B101 was taken from basal continental alluvial to lacustrine clastics adjacent to the Bukulja Mountains (the Aranđelovac Miocene Basin, Figs. 5a, 7b). Both ZFT and AFT analyses do not pass the χ^2 test. The sample yielded mean ZFT age of 22.7 ± 2.6 Ma. Statistical decomposition of age distributions in sample B101 yielded two best-fit ZFT peak ages of 18 Ma and 48.1 Ma, with both zircon components consisting of grains with rounded morphologies (Fig. 10a, Table 1). Additional calculation using the χ^2 age method yielded the pooled age of the youngest zircons fraction of 18.0 ± 1.3 Ma, which indicates the oldest time when the deposition of this sample could have occurred (Fig. 10a). Furthermore, statistical decomposition of apatite fission track age distributions in the same sample B101 yielded two best-fit AFT peak ages of 16.2 Ma and 33.6 Ma (Fig. 10a, Table 2). The combined 18–16 Ma ages indicate rapid exhumation of the source area that continued until the similar age of deposition (~16–15 Ma). The older age populations of

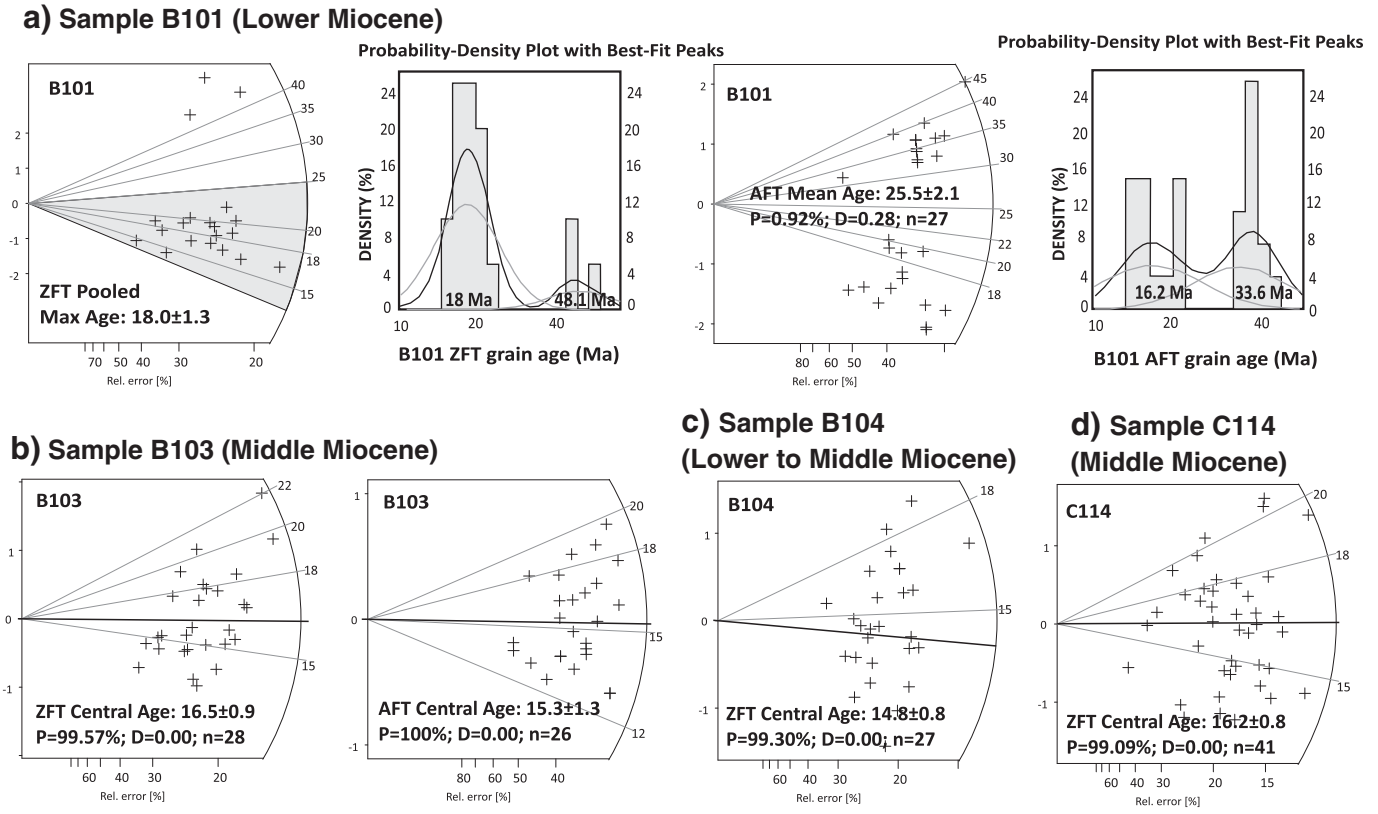

Fig. 10. ZFT and AFT detrital thermochronology of samples from the Bukulja and Cer Mountains. The radial plots representing ZFT and AFT single grain age distributions were obtained using the TrackKey software (Dunkl, 2002). Central ages of the samples are indicated by solid black lines, and the youngest age populations for heterogeneous samples are indicated by grey shaded areas. Probability-Density Plots with Best-Fit Peaks for heterogeneous samples were obtained using the BinomFit software (Brandon, 2002). Abbreviations: n- number of grains counted; Ages are central ages, unweighted mean ages, or pooled ages of the youngest age population; P—probability obtaining Chi-square (χ^2); D—dispersion in single grain ages.

ZFT 48 Ma and AFT 33 Ma indicate cooling in the source area during Eocene–Earliest Oligocene times.

In the same basin, but a higher Middle Miocene stratigraphic interval, sample B103 (Figs. 5a, 7b) pass the χ^2 test for apatite and zircon fission track analyses. These are, in both cases, provenance ages. ZFT central age of 16.5 ± 0.9 Ma in sample B103 is associated with a homogeneous age distribution, with euhedral morphologies of zircon grains pointing to a magmatic source and short duration of transport and sedimentation. AFT central age of the same sample is 15.3 ± 1.3 Ma (Fig. 10b). Measured mean track length (MTL) value is 14.14 ± 1.13 μm, while the average D_{par} has the value of 1.3 ± 0.2 μm (Table 2). Close range ZFT and AFT ages coupled with high values of measured MTL (Table 2) indicate fast Middle Miocene cooling in the source area.

Sample B104 represents late Early to early Middle Miocene shallow-water coarse clastics collected from the southern flank of the Bukulja Mountains (Belanovica Basin, Fig. 5a). The obtained ZFT central age of this sample has the value of 14.8 ± 0.8 Ma and passes the χ^2 test, while the grains expose euhedral morphologies and can be associated with a magmatic source area (Fig. 10c, Table 1).

One sample C114 has been collected in the coarse clastics that mark the onset of the Middle Miocene transgression over the southern flank of the Cer Mountains (Jadar Basin, Figs. 4a, 7c). This sample yielded a provenance ZFT central age of 16.2 ± 0.8 Ma passing the χ^2 test with a homogeneous age distribution, while the zircon grains with euhedral morphologies infer a short range transport from a magmatic source area (Fig. 10d, Table 1).

4. Zircon U—Pb geochronology of the Cer and Bukulja granitoids

In order to set temporal constrains on emplacement of the Cer and Bukulja granitoids, new LA-ICPMS U—Pb zircon geochronology of five samples was conducted at the Laserchon Facility, University of Arizona, USA. The detailed analytical procedures are presented in Appendix B. In the Cer Mts one sample (Cer1, Fig. 4) was analyzed from an intrusion of granodiorites to quartz-monzonites in the Stražanica area, while two other samples were analyzed from the I-type quartz-monzonite located in the core of the mountains (Cer3 and Cer4, Fig. 4). In Bukulja two samples were analyzed from the S-type two-mica granite situated in the core of the mountains (Buk1 and Buk4, Fig. 5).

In sample Cer1 29 core and rim individual U—Pb zircon determinations were conducted. 15 out of 29 grains yielded different core and rim ages, with cores being older to significantly older than the rims. These older core grains were interpreted as inherited grains with ages ranging between ~600 and 40 Ma. The remaining 14 cores as well as all rims yielded concordant Early Oligocene ages that were used to determine an average 238 U/206Pb age of 31.92 ± 0.67 Ma (MSWD = 2.8), which was interpreted as the crystallization age of the Stražanica granodiorite (Fig. 11). In case of sample Cer4 10 out of 26 grains yielded different core and rim ages, and were interpreted to represent inherited grains with ages ranging between ~487 and 87 Ma, whereas the remaining 16 cores and rims yielded concordant ages that allowed for determination of an average 238 U/206Pb age of 31.36 ± 0.49 Ma (MSWD = 2.0), interpreted as the crystallization age of the main body of the Cer Mts quartz-monzonite. Very similar average 238 U/206Pb age of 32.21 ± 0.30 Ma (MSWD = 1.4), again interpreted as the age of crystallization was obtained on another Cer Mts quartz-monzonite sample Cer3 (Fig. 11). Here all 24 grains yielded concordant Early Oligocene core and rim ages that were pooled to determine an average 238 U/206Pb age. In the case of Bukulja Mts two-mica granite sample Buk1, 19 core and rim individual U—Pb zircon determinations were carried out. All 19 grains yielded concordant Late Oligocene to Early Miocene core and rim ages, used to determine an average 238 U/206Pb age of

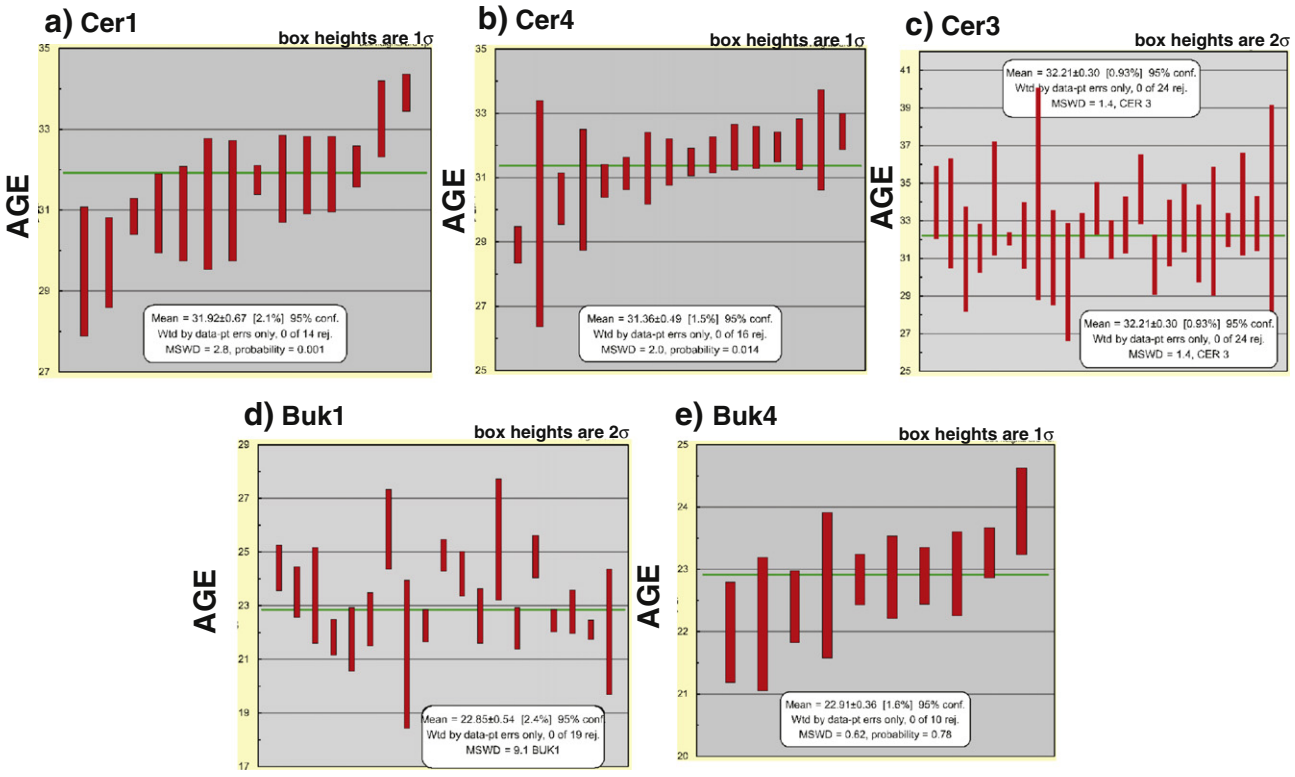

Fig. 11. ^{238}U—^{206}Pb pooled crystallization ages of samples a) Cer1, b) Cer4, c) Cer3, d) Buk1, and e) Buk4.

22.85 ± 0.54 Ma (MSWD = 9.1) that was again inferred as the crystallization age of this rock (Fig. 11). Similar ages were obtained on another two-mica granite sample Buk4. 4 of the analyzed zircon grains yielded different core and rim ages, and were interpreted as inherited grains with ages ranging between ~250 and 41 Ma. The remaining 10 grains gave concordant Early Miocene core and rim ages that allowed for determination of an average 238 U/206Pb age of 22.91 ± 0.36 Ma (MSWD = 0.6). This age was interpreted as the crystallization age of the Bukulja Mts two-mica granite (Fig. 11).

All U—Pb zircon ages obtained on the Cer Mts quartz-monzonite and granodiorites bodies cluster at ~32 Ma and are interpreted as crystallization ages that mark the time of their emplacement. Hence, previous K—Ar ages spanning between 21 and 15 Ma actually represent cooling ages, resulting from rapid tectonic exhumation in the core of

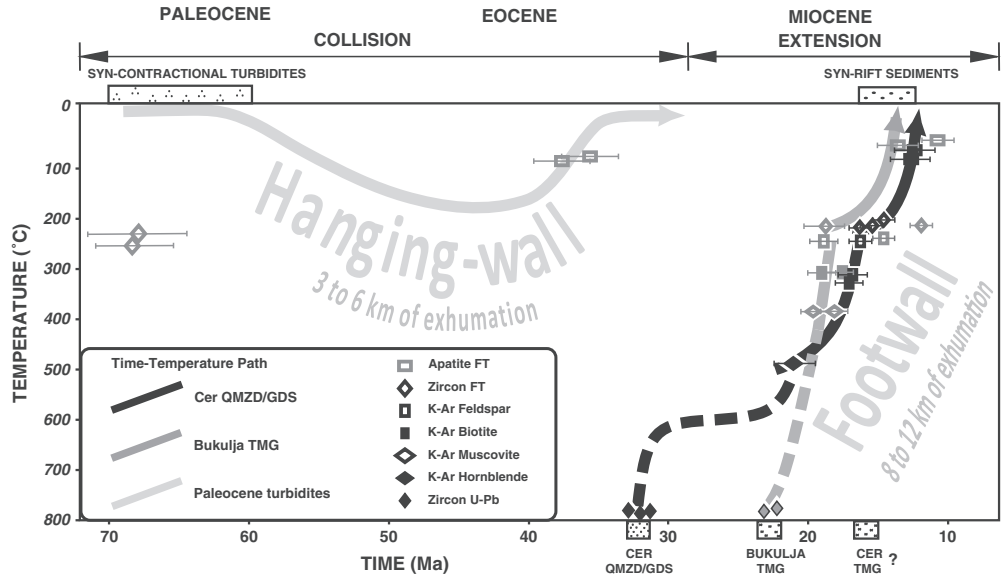

Fig. 12. Contrasting thermal histories of rocks that comprise footwall and hanging-wall units of the Cer and Bukulja Mountains core-complexes. Temperature-time diagram was constructed by using ZFT ages, AFT ages, and modeled t-T paths of Paleogene turbidites samples Cer6 and B105; U—Pb zircon ages, ZFT ages, AFT ages, and modeled t-T paths of quartz-monzonite/granodiorite and two-mica granite samples Cer1, Cer3, Cer4, Buk1, Buk4, as well as the available K—Ar ages from Cer and Bukulja plutons (Cvetković et al., 2007; Knežević et al., 1997; Koroneos et al., 2011; Stojadinovic et al., 2013).

the Cer Mts during Early to Middle Miocene times. This inference is supported by the fact that the K—Ar ages are in range of ZFT ages obtained in the same magmatic bodies (Figs. 4a, and 12, see also Stojadinovic et al., 2013). In the case of Bukulja Mts two-mica granite U—Pb crystallization ages cluster at ~23 Ma (Fig. 5a) thus indicating that the emplacement of this body occurred in the lowermost Miocene. Scattered 20–15 Ma K-Ar ages should be regarded as result of continuous Miocene cooling/exhumation of the pluton following its magmatic emplacement (Fig. 12, see Stojadinovic et al., 2013).

5. Source areas and evolution of the Uppermost Cretaceous–Paleocene *syn*-kinematic sediments

The fission track thermochronological analysis of the Upper Cretaceous–Paleogene sediments situated at or near the contact between European and Adriatic- derived units of the Dinarides demonstrate a consistent history of rapid cooling in the source area combined with episodes of burial and followed by exhumation, erosion, transport and deposition. This Late Cretaceous–Paleogene tectonics postdates more scattered older tectonic episodes.

ZFT measurements of sample B105, representing turbidites of the eastern flank of the Bukulja Mountains in the hanging-wall of the Miocene detachment (Fig. 5a) show two older single grain age populations of 200.7 Ma and 107.1 Ma (Fig. 8c; Table 1). None of these ages can be directly related to tectonic events previously interpreted in the study area. The older Late Triassic (Norian) age can only be ascribed to the Middle Triassic volcanism associated with the opening of the Neotethys in the Dinarides that is known to have locally continued during Late Triassic times in other regions of the Dinarides (Gawlick et al., 2009; Missoni et al., 2012; Pamic, 1984). This is consistent with the observations of various volcanic sequences interpreted as Middle Triassic that were metamorphosed in the distal part of the Jadar-Kopaonik units and subsequently exhumed in the footwall of Miocene extensional detachments (Erak et al., in this issue; Schefer et al., 2010; Toljić et al., 2013). This may represent a source area for the 200 Ma ZFT population, although the areal extent of such rocks is quite limited. The late Early Cretaceous (intra-Albian) population corresponds to contractional events recorded in both the Dinarides and neighboring Carpatho-Balkanides. In the Dinarides, kinematic, exhumation and provenance studies have inferred a significant contractional event in the region of the Medvednica Mountains of Croatia, near the junction with the Eastern Alps (Lužar-Oberiter et al., 2012; Tomljenovic et al., 2008; van Gelder et al., 2015). One late Early Cretaceous metamorphic age has been inferred in the area of the Kopaonik Mountains, south of our studied area (Schefer, 2010). In contrast, the late Early Cretaceous tectonics had much larger effects on the European side neighboring our study area. Intra-Albian is the proposed period when the Supragetic nappe of the Carpatho-Balkanides was thrusted over the Getic units, an effect of the collision following the closure of the Ceahlau-Severin ocean in the South Carpathians (Iancu et al., 2005). This event is continuous along the strike of the neighboring Serbian Carpathians and is compatible with the late Early Cretaceous event detected by metamorphic burial ages and post-tectonic covers in the along-strike prolongation in the Kraishte window of SW Bulgaria (Kounov et al., 2010). Late Early Cretaceous exhumation ages within large error bars (~15 Ma) have been detected by fission track studies of the Serbo-Macedonian unit of southern Serbia, interpreted as extensional detachments affecting the European margin adjacent to the Sava suture zone (Antić et al., 2015). Late Jurassic–Early Cretaceous K—Ar cooling ages on muscovite and K-feldspar were obtained in the northernmost exposed parts of the Serbo-Macedonian unit in central Serbia (Fig. 1a, Balogh et al., 1994), although these ~155–125 Ma ages are significantly older. It is likely that our limited population of late Early Cretaceous provenance ages are derived from the exhumation associated with one of these tectonic events on the European side, although their distribution and significance still remains to be largely quantified in central and southern Serbia.

5.1. Late Cretaceous–Paleocene source areas

In contrast to the above more speculative interpretation, the Late Cretaceous–Paleogene history of our samples is better constrained. All our detritic samples, either from uppermost Cretaceous–Paleocene or from Miocene sediments, contain detrital ZFT central ages or populations concentrated at ~70–64 Ma along the flanks of all three studied areas of Bukulja, Cer and Fruška Gora Mountains (Figs. 8–10). Interestingly, in all of the uppermost Cretaceous–Paleocene samples the stratigraphic age is very close or even overlaps within its error bars with the ZFT age populations. This means that extremely fast exhumation, transport and deposition has occurred in a nearby source area, or, alternatively, zircons cooled within a volcanic (or intrusive) source were rapidly transported to the trench accumulating turbiditic sediments during coeval contraction.

A stage of latest Cretaceous contractional exhumation of the Serbo-Macedonian and Supragetic units adjacent to the study area at ZFT resolution is largely unknown. This is also unlikely because sediments of various Cretaceous ages are still preserved and overlying the Serbo-Macedonian upper tectonic unit of the Dinaridic subduction system in various positions along the strike of the chain (Fig. 1). If Latest Cretaceous exhumation at ZFT resolution has taken place, then it should have affected only the central part of this unit at farther distanced from the study area, where sediments of this age are missing. This contrasts with the inferred coeval age of the collision and significant deformation recorded by the turbiditic trench sediments (Schmid et al., 2008; Ustaszewski et al., 2010).

Late Cretaceous populations contain zircons with euhedral morphologies, supporting the volcanic/magmatic source hypothesis. This is fully consistent with the widespread Late Cretaceous magmatism observed in European units. The long along-strike belt of intrusive and extrusive magmatism in the Apuseni, Banat, Timok, Panagyurishte and Eastern Srednogorie took place between ~92–67 Ma (Gallhofer et al., 2015 and references therein). These studies showed that the Timok segment adjacent to our study area (Fig. 1b) started to be active between 90 and 87 Ma and ended at around 74–71 Ma. These ages are a few Ma older, than our provenance clusters. In much smaller observed volumes, a second magmatic source can be represented by the latest Cretaceous–Paleocene (72–53 Ma) alkaline magmatism (Cvetković et al., 2013) observed in closer proximity to our study area, although the potential importance of these rocks as a source for zircons is clearly reduced.

Although the bulk of biostratigraphic dating in the turbiditic sequences of Bukulja, Cer and Fruška Gora Mountains inferred narrow Maastrichtian ages, it is rather clear that their deposition went into Paleocene times, while the lower continental to shallow water transgressive part is locally older (Čanović and Kemenci, 1988; Marović et al., 2007). The Paleocene stratigraphic ages of our samples (~60 Ma) result in a lag time of ~5 to 10 Ma between volcanic emplacement or exhumation beneath ZFT temperatures and sedimentation in the trench.

5.2. Burial and Late Eocene exhumation

Postdating their deposition in Late Cretaceous–Paleocene times, the AFT ages in the sediments flanking the Cer and Bukulja Mountains show quite homogenous central ages at ~40–34 Ma (samples Cer6 and B105, Figs. 4, 5, 8). When combined with their kinetic parameters and thermal modelling, this indicates a thermal overprint of these sediments by burial after deposition and exhumation in Middle to Late Eocene times (Fig. 8). This can be translated to 3–6 km of coeval exhumation. Furthermore, similar provenance ages are observed in populations of the Miocene sediments flanking the Bukulja and Fruška Gora structures (sample B101 and F120, Figs. 3, 5, 9, 10). Note that the exhumation of these rocks situated in the hanging-wall of the Miocene detachments reflects a different history when compared with the ones in their footwall only a few kilometers away, which reflect the cooling during Miocene exhumation (Figs. 4, 5, and 12, see also Stojadinovic et al., 2013). A

similar tectonic exhumation could have taken place also in the Fruška Gora Mountains. However, the Middle – Late Eocene tectonic episode has been completely overprinted in this area by enhanced erosion as a result of the subsequent tectonically induced Miocene exhumation (sample Fg4, Fig. 8a). The Middle–Late Eocene exhumation is preserved only as provenance ages in the Miocene sediments flanking the Fruška Gora (sample F120, Fig. 3).

This new finding of Paleocene–Middle Eocene burial and Middle–Late Eocene exhumation demonstrates that large amounts of contraction took place in the NE Dinarides at their contact with the European upper tectonic plate after a significant time following the onset of collision in the Latest Cretaceous. No coeval marine sedimentation of Middle-Late Eocene age is recorded in the studied area, most likely due to complete exposure to continental conditions or subsequent removal by erosion. Therefore, such contraction is difficult to date without AFT resolution thermochronological data, which is lacking in the European-derived units (Serbo-Macedonian and/or Supragetic) neighboring our area. The stage of Middle–Late Eocene contractional driven exhumation can be correlated with the Eocene age of metamorphism (~45–35 Ma) dated by Ar—Ar isotopic analysis in the in the Studenica window of Central Serbia, south of our studied area (Fig. 1b, Schefer, 2010). Our AFT ages are also compatible with observations west of our studied area, where Late Eocene fission track cooling ages were obtained in the Late Cretaceous–Paleogene turbiditic sediments in the Kozara Mountains of northern Bosnia, interpreted to be a result of hanging-wall erosion during thrust propagation into the external Dinarides since around 40 Ma (Ustaszewski et al., 2010). These ages are indeed coeval with the Middle–Late Eocene phase of shortening that is widely observed in the External Dinarides, extending as far west as the Southern Alps (i.e. the Dinaric phase, Channell and Doglioni, 1994; Schmid et al., 2008). Our results suggest burial and subsequent exhumation by erosional unroofing and, therefore, infer a more continuous contractional evolution.

6. Miocene re-sedimentation in close proximity of rapidly exhuming source areas

The results of our detrital thermochronology study clearly indicate a Miocene event of fast exhumation observed in both exhumation and provenance ages, either central ages that passed the χ^2 test or in age populations obtained by statistical decomposition. This is most clearly observed in the previous exhumation ages in the core of the Bukulja and Cer Mountains (Stojadinovic et al., 2013) combined with newly obtained provenance ages in this study along their flanks. In these areas, Early to Middle Miocene *syn*-rift sediments and their AFT and ZFT provenance ages (Figs. 1b, 4, and 5), demonstrate typical features of rapid exhumation, transport and short-range deposition occurring within asymmetric extensional basins.

Along the northern flank of the Bukulja Mountains, the ~17–15 ZFT and AFT provenance ages obtained in the Miocene sediments are within the range of the ~19–10 exhumation ages obtained in the metamorphic footwall of the main detachment (Figs. 5a and 7b). The exhumation related to the extension started earlier at ~23 Ma, as inferred from the U—Pb zircon age of the central extensional-related pluton. The provenance ages are fairly close and within the error bar of the depositional age that cannot be older than ~15 Ma, somewhere near the transition between Lower and Middle Miocene where massive coarse clastics (the Bučvar coglomerates of Dolić, 1997) mark the first stage of the gradual opening of the Central Paratethys to marine conditions. The estimated lag time between exhumation beneath ZFT resolution and sedimentation is in the order of 2–3 Ma. When combined with the rounded morphologies of zircon grains and apatite track length characteristics of sample B101, this demonstrates very fast exhumation of the footwall of the Bukulja metamorphic core that provided the source for the Miocene sediments (Fig. 5, Table 2, see also Stojadinovic et al., 2013). Same observations can be made for sample B103, although euhedral morphologies of zircon grains showing no evidence of abrasion point to the nearby pluton as the direct source area, which has undergone rapid Miocene tectonic cooling with average rates of 50 °C/Ma, postdating its magmatic emplacement at ~23 Ma (Figs. 5a, 12, Stojadinovic et al., 2013). South of the Bukulja Mountains, the provenance ZFT age of 14.8 ± 0.8 Ma of coarse clastic sample B104 (Belanovica Basin, Fig. 5a) combined with some euhedral morphologies may indicate the northern pluton as the source area. But several other sub-volcanic intrusions, along with associated volcanics and volcaniclastics, associated with the Pannonian extension occur south of the Belanovica Basin (Figs. 2a and 5a) and might provide the required source area (Cvetković et al., 2007; Filipović et al., 1976).

Similar inferences are derived from the late Early Miocene ZFT provenance age ~16 Ma from the Jadar Basin south of the Cer Mountains (Fig. 4a). This sample indicates a homogeneous distribution of single-grain zircon ages that coupled with observations of euhedral grain morphologies allows us to assign the adjacent Cer Mountains pluton as the source area, which was rapidly exhumed in the Middle Miocene in the footwall of the main detachment with average rates of ~50 °C/Ma (Figs. 2, 4, 12, Stojadinovic et al., 2013). This has provided the source for the Middle Miocene marine clastics deposited in the south (i.e., in the Jadar Basin, Fig. 4a).

The situation is slightly different in the Fruška Gora. This is illustrated at best by the Uppermost Cretaceous–Paleocene sample Fg4 (Fig. 8a) that shows a provenance ~71 Ma population age and one other exhumation ~11 Ma population age. This means that this sample received zircons from source area with ~71 Ma cooling age during its deposition and has been subsequently buried and ultimately rapidly exhumed during the late Middle Miocene by a tectonic event. The burial was above the AFT but below the ZFT resolution, which means 3–6 km. Previous structural and exhumational studies of Fruška Gora (Fig. 3a) have inferred that the main exhumation of the SW located metamorphic core took place during Late Oligocene–Early Miocene in the footwall of the main extensional detachment and was followed by a Middle–Late Miocene second stage of extensional exhumation of the entire mountains (Stojadinovic et al., 2013; Toljić et al., 2013). Our higher resolution study is able to refine this hypothesis and infer that the second stage of exhumation has affected only the metamorphic core and the pre-Miocene sequence of Fruška Gora in the hanging-wall of the main detachment at AFT resolution.

All other ages on the farther flanks of the mountains are provenance ages and, similarly with the Bukulja and Cer Mountains, demonstrate a rapid phase of tectonic exhumation in a source area situated in their proximity. This is demonstrated best by the coherent full set of Early Miocene ZFT, AFT and AHe ages (~24–19 Ma, from ~250 °C to 70 °C) of the upper Lower Miocene sample Fg6 combined with a high value for the track length measured in apatite grains and a narrow length distribution (Table 2). A similar provenance age of ~24 Ma is also observed in sample F117. When combined with the close Lower Miocene stratigraphic age, it demonstrates a rapid tectonic event taking place in the metamorphic core of the Fruška Gora situated in its proximity (Fig. 3). Given the high geothermal gradient at the time of the Pannonian extension (presently ~40 ± 10 °C/km, Adam and Wesztergom, 2001; Lenkey et al., 2002) this infers 4 to 6 km of exhumation of the Fruška Gora metamorphic core in the Early Miocene. When taking into account the ~29 Ma Rb—Sr Late Oligocene age in the metamorphic core (~400 °C, Toljić et al., 2013), this infers a minimum of 7–10 km of exhumation during the Late Oligocene–Early Miocene in the footwall of the main Fruška Gora detachment.

The second stage of Middle to Late Miocene exhumation between ~16–10 Ma (Stojadinovic et al., 2013) is well documented by provenance ages in both ZFT and AFT data in all other new samples (FG4, F118, F120, Fig. 3a). High values for the track length measured in apatite grains and a narrow length distribution (Table 2) combined with the close stratigraphic age (e.g., F118, F120) demonstrate another rapid tectonic event taking place in the metamorphic core and the pre-Miocene

rocks of the Fruška Gora situated in its proximity. Interestingly, the ZFT provenance age of ~12 Ma in sample F118 infers that the exhumation was locally much higher in the center of the structure than the previously inferred 2–4 km during the second exhumation stage (Stojadinovic et al., 2013), being at least 5–7 km given the Pannonian Basin geothermal gradient. It should have rapidly decreased towards its flanks where only older provenance ZFT ages are observed.

7. Discussion

Our study infers a more complex mechanics of continental collision between Europe- and Adria- derived units during the closure of the Neotethys Ocean in the NE Dinarides when compared to the rather simple assumption of the formation of one suture zone during latest Cretaceous times followed by prolonged minor deformation during the Paleogene (e.g., Schmid et al., 2008; Ustaszewski et al., 2010 and references therein). In terms of exhumation the situation in the studied area is exactly the opposite. The latest Cretaceous–Paleocene exhumation was minor at least in the areas neighboring our study, while prolonged contraction with larger burial and exhumation was effective throughout the Eocene.

Most of the zircons in the sediments deposited in the trench situated at the contact between the two plates were shed from slightly earlier (2–10 Ma) emplaced magmatic sources, most likely from the volcanic

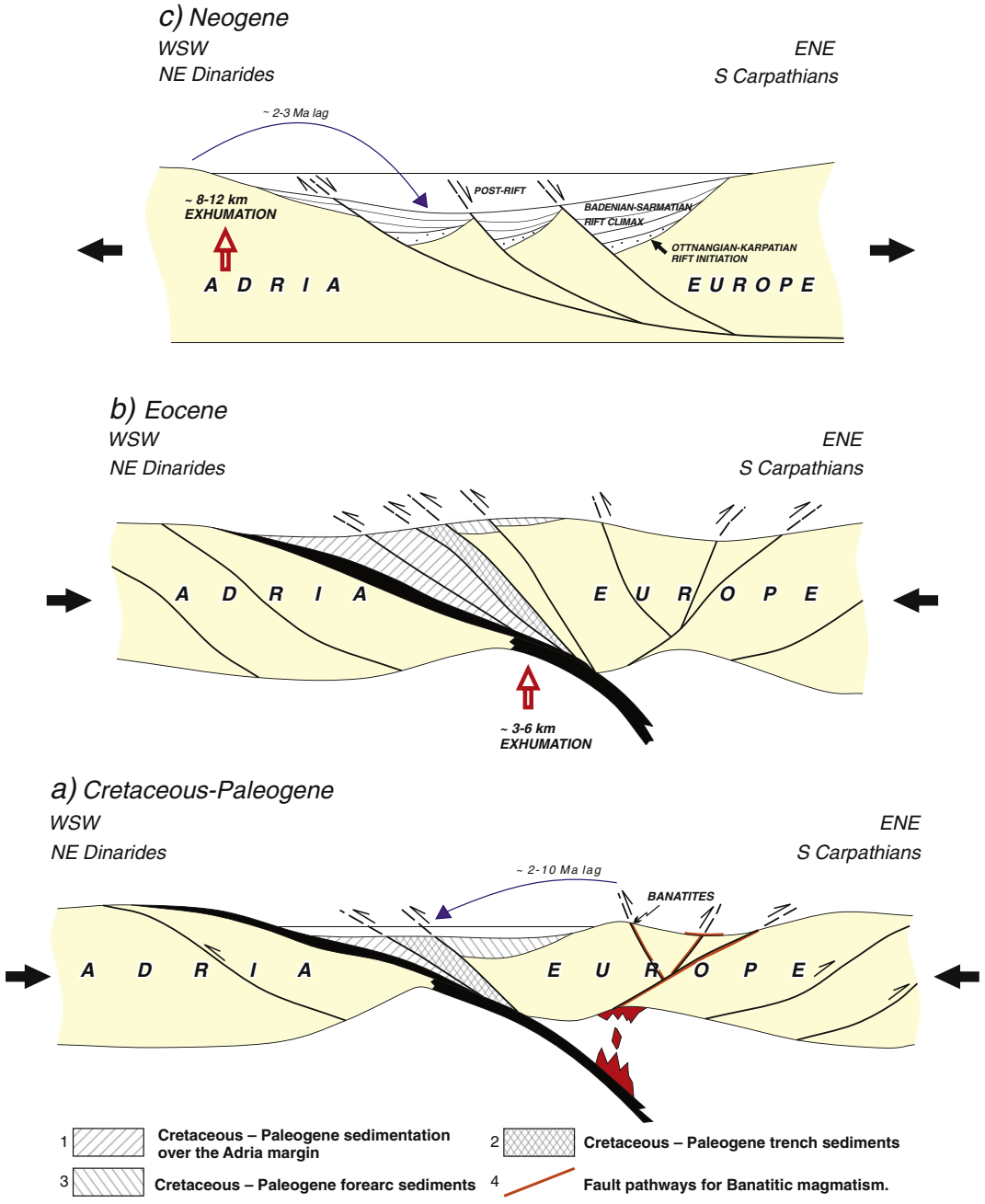

Fig. 13. (concluding): Late Cretaceous to Miocene tectono-sedimentary evolution of the NE Dinarides margin. a—Latest Cretaceous–Paleogene (between ~75 and 60 Ma): collision of the Carpathians units with the Dinaridic margin led to the deposition of *syn*-contractional trench turbidites of the Sava suture (after Schmid et al., 2008), which overlie the older Cretaceous sedimentary succession. "Sava" turbidites contain predominantly a magmatic source area derived from the neighboring "banatites"; b—Middle to Late Eocene (between ~45 and 35 Ma): gradual shortening through the Paleogene resulted in burial of the trench sediments, followed by 3 to 6 km of exhumation in the turbiditic basin during the Middle–Late Eocene phase of contraction; c—Miocene (between ~24 and 12 Ma): 8 to 12 km of Early to Late Miocene exhumation of the Dinarides margin in the footwalls of extensional detachments, followed by Ottnangian–Karpatian to Badenian–Sarmatian syn-rift deposition (after ter Borgh, 2013).

structures and sub-volcanic intrusions of the neighboring Timok area (Fig. 1b). This area must have been a topographic high at the time of emplacement, either along the main (magmatic) arc or slightly in the back-arc, uplifted likely during active rifting (sensu Ziegler and Cloetingh, 2004), which accompanied the emplacement of large calk-alkaline volcanic volumes (see also Gallhofer et al., 2015; von Quadt et al., 2005). Given the lag time and the youngest ~64 Ma age population of our ZFT data, the sedimentation in the trench certainly spanned well into the Paleocene. In the vicinity of the subduction trench, the European upper plate (Serbo-Macedonian unit) was covered by widespread coeval sedimentation recorded along the strike of the Dinarides at least from the regions east of Fruška Gora to south of the studied area (Fig. 1b, Čanović and Kemenci, 1988; Matenco and Radivojević, 2012; Toljić, 2006). Outcrop and well observations suggest that these sediments were deposited in a forearc basin overlying the frontal part of this plate, which experienced extension during the early onset of the magmatism (Turonian–Campanian) and significant contraction afterwards that spanned into the early Paleogene (Toljić et al., 2013). Due to lack of thermochronological data in the intervening Serbo-Macedonian unit, we cannot completely exclude significant latest Cretaceous–Paleocene exhumation in the European plate area situated between the forearc sedimentation and the main Timok magmatic arc (Fig. 1b). Such exhumation may be inferred by the minor rounded zircon population observed in our study. Depending on the assumed geothermal gradient, it should have been in the order 6–12 km.

After the latest Cretaceous–Paleocene contraction, the sediments of the trench were buried beneath the European margin at depths of about 4–6 km and rapidly exhumed during a Middle–Late Eocene event (Fig. 12). Both burial and exhumation must have been contractional. Many of the thrust fault or unit contacts observed in or near the Sava suture zone and previously assumed to have formed during the latest Cretaceous–Paleocene must be, in fact, Middle–Late Eocene in age. In fact, the contraction continued throughout the latest Cretaceous–Late Eocene, which is the age of the collision as a contractional on-going process. The 4–6 km of exhumation during the Middle–Late Eocene infers also that the trench and forearc basins sediments were deposited over much larger areas during the latest Cretaceous–Lower Eocene, possibly accommodating sedimentation that was removed afterwards by exhumation and erosion. Such Paleocene–Eocene *syn*-kinematic contractional sedimentation is observed along the strike of the Sava Zone in neighboring NW Bosnia and Herzegovina and adjacent area of Croatia, although the effects in terms of contractional exhumation are likely lower (Hrvatović, 2006; Ustaszewski et al., 2010). The switch from burial in the studied area of the Sava zone to Middle–Late Eocene exhumation (~34–37 Ma) is likely related to a more regional process, as the latter effect and associated contractional deformation is observed in various locations in the Dinarides across its entire strike (e.g., Channell and Doglioni, 1994; Schmid et al., 2008; Ustaszewski et al., 2010; van Gelder et al., 2015). Whether this has anything to do with post-dating deep Dinaridic slab processes, such as delamination or slab roll-back (Schefer et al., 2011), resulting in a switch in deformation mechanics, is beyond the scope of our study. Post-dating the Middle–Late Eocene peak in contractional deformation, such contraction has been observed to continue only during the latest Miocene–Quaternary times at the scale of the entire Dinarides (e.g., Pinter et al., 2005 and references therein), although it could have continued with significant offsets in the SE external Dinarides of Montenegro (e.g., Bennett et al., 2008).

8. Conclusions

Our detrital provenance thermochronological study of the NE Dinarides in the critical areas neighboring the Fruška Gora, Bukulja and Cer Mountains near or at the Latest Cretaceous–Paleogene collisional contact between Europe- and Adriatic- derived units has demonstrated a more complex tectonic evolution than the previously inferred simple formation of a suture zone. The Latest Cretaceous–Paleocene trench was supplied by sediments from a predominantly a magmatic source area originating in the neighboring Timok magmatic arc which must have formed an elevated topographic high at those times (Fig. 13a). While the upper plate European margin adjacent to the trench was covered by a forearc basin whose evolution changed in time from extensional to contractional, no significant exhumation is inferred at farther distances in this upper plate, or such exhumation has affected only limited intervening areas towards the magmatic arc. The trench and neighboring areas were subsequently buried by the contraction and were ultimately exhumed during the Middle–Late Eocene from below a 4–6 km overburden that was removed by erosion during the coeval contraction (Fig. 13b). This latter event is regional and it took place at the scale of the entire Dinarides, likely by the activation of out-of-sequence thrusts in their internal areas. Such deformation is difficult to discriminate by other means than thermochronology due to the coeval erosional removal of eventual syn-kinematic sediments either during the later contractional event or during the subsequent extension.

The internal Dinarides were affected by large scale extension during Late Oligocene–Miocene times by the formation of numerous extensional detachments that exhumed previously buried distal Adriatic and Sava suture rocks in their footwall. Our study demonstrates that this exhumation created multiple and very dynamic source areas that were rapidly exhumed, eroded and shed sediments in a matter of a couple Ma over short distances in the adjacent Miocene basins (Fig. 13c). This dynamic source was either stable and localized in the footwall of the detachment, such as in Bukulja or Cer Mountains, or gradually enlarged at local scale in their hanging-wall, such as observed in Fruška Gora. Both situations document fast exhumation and short range transport in the immediate basins of detachment hanging walls. Such local basin formation and rapidly eroding footwalls as the immediate source area is similarly observed or discussed elsewhere at the scale of the entire Pannonian basin (e.g., Horváth et al., 2015; Matenco and Radivojević, 2012; Tari et al., 1992, 1999). This is a mechanism well known in major extensional provinces controlled by series of detachments forming shallow asymmetric basins, such as the Basins and Range of the western US (e.g., Wernicke, 1992).

Overall, the results of our study point to particular kinematics, in which the onset of collision has resulted in minor exhumation of the upper tectonic plate. This upper tectonic plate recorded such significant exhumation only during the very late stages of collision, after ~30 Ma time interval. The latter has affected the orogen on a much broader scale and was subsequently followed by the onset of extension in the internal part of the orogen, including the accreted lower plate, while the more external parts recorded contraction. Such a mechanisms of collision that involves an initial gradual accretion by contraction followed by out-of-sequence thrusting and extension in the internal parts of the orogen is a typical characteristic of many other Mediterranean orogens dominated by slab-retreat, such as the Carpathians, Apennines, Ligurian Alps or the Betic-Rif system (Bertotti et al., 2006; Matenco et al., 2016; Picotti and Pazzaglia, 2008; Vergés and Fernàndez, 2012). What makes the Dinarides special is the extreme non-exhumation of the orogenic core during the onset of collision which must have been driven rather by deep mantle processes than near-surface crustal deformation.

Acknowledgements

This study is a result of the collaboration between Utrecht University, The Netherlands and Faculty of Mining and Geology, University of Belgrade, Serbia and was funded by the Netherlands Research Centre for Integrated Solid Earth Science (ISES) during the PhD study of Uros Stojadinovic. The authors acknowledge excellent comments and suggestions of the reviewers Kamil Ustaszewski and Borna Lužar-Oberiter. Stefan Schmid is acknowledged for discussions in understanding the evolution of the Dinarides. Vladica Cvetković is gratefully acknowledged for discussions on the Dinarides magmatism.

Appendix A. Zircon and apatite fission track thermochronology

An average of ~5–6 kg of rock was collected per sampling location. Apatite and zircon mineral separation, including crushing, sieving, heavy liquid and magnetic separation, followed standard procedures at VU Amsterdam, The Netherlands (e.g., Foeken, 2004). Irradiation of zircon and apatite mounts prepared using the detrital samples was performed at FRMII Garching (Technische Universität München, Germany). Zircon mounts were irradiated together with zircon age standards (Fish Canyon Tuff 27.9 ± 0.7 Ma, Tardree Rhyolite 58.7 ± 1.1, and Mt. Dromedary Banatite 98.7 ± 0.6 Ma; Garver, 2003) and reference glass dosimeters CN-1 and CN-2. Apatites were irradiated along with apatite age standards (Fish Canyon Tuff 27.9 ± 0.7 Ma, Durango 31.4 ± 0.5 Ma, and Mt. Dromedary Banatite 98.7 ± 0.6 Ma; Green, 1985) and reference glass dosimeters CN-2 and CN-5. Prior to the irradiation apatite grain mounts were etched with 1.5 N HNO3 at 21 °C for 35 s. Zircons grain mounts were etched in a eutectic mixture of KOH and NaOH at 225 °C for 16 to 52 h. After irradiation, the external mica detectors and reference glass dosimeters were etched in 48% HF at 21 °C for 12 and 25 min, respectively, in order to reveal the induced tracks. Densities of spontaneous and induced tracks in zircon and apatite grains were determined using an Olympus BX51 microscope with a magnification of 1000× equipped with a computer controlled Autoscan® System (Autoscan System Ply. Ltd. 2002). Apatite and zircon grain mounts were dated by the external detector method (EDM; Gleadow and Duddy, 1981). Fission track ages are reported with statistical uncertainties quoted at the ±1σ level, using zeta factor of 349 ± 15 (apatite, CN5 glass) and 134 ± 5 (zircon, CN1 glass) (analyst Uros Stojadinovic).

The most important factors in detrital zircon fission-track measurements are spontaneous track density, fission-track cooling age, and uranium content, which together define a "window of countability" for detrital zircon (Bernet et al., 2004). Under-etched or over-etched grains, grains with very high spontaneous track densities, strong zonation, or very small counting areas of <500 μm^2, were not included. Detrital apatite, when not exposed to increased temperatures, retains fission tracks formed prior to deposition and fission tracks formed after deposition. Therefore, in cases when apatite fission-track ages are older than the stratigraphic age of the measured sample and form a homogeneous distribution of single grain ages, fission track length are measured (confined horizontal tracks and long axes of etch pits). Considering tracks found in the detrital apatite grains as provenance-related tracks, that were formed and annealed during pre-depositional cooling, we linked the track length data with the corresponding fission track ages. On the other hand, when all other components of the provenance system are known, detrital single-grain age populations may constrain a stratigraphic age that is unattainable by other methods. In this case, the youngest single age in a multiple FT population marks the maximum age of deposition, assuming that heating during the burial can be excluded.

Whenever samples had a P (χ^2) value of <5%, it indicated the presence of more than one age component (Tables 1 and 2). Therefore, decomposition of these samples was conducted using the BinomFit software (Brandon, 2002). From the attained age distributions, single age components are derived by fitting to a set of Gaussian distribution functions (Gaussian peak-fitting method, Brandon, 1992). In addition, the χ^2 age method (Brandon, 1992) was applied to isolate the youngest of the zircon fission track single grain age component in the given sample. The χ^2 age is defined as the pooled age of the largest group of young grains that still retains P (χ^2) >5%. P (χ^2) is calculated using the TrackKey software (Dunkl, 2002). Horizontal confined track measurements, as well as the etch pit diameter (D_{par}) measurements were performed on the same apatite grain mounts. Time-temperature histories of the samples were modeled using HeFty programme (Ketcham et al., 2003). Integrated AFT age data, track length distributions, and etch pit diameters (D_{par}) were used as input parameters, whereas the obtained ZFT ages provided additional constrains for the models. Zircon closure temperature was constrained to 250 ± 50 °C and zircon partial annealing zone (ZPAZ) to 300–200 °C (Tagami, 2005). Apatite closure temperature was constrained to 110 ± 10 °C and apatite partial annealing zone (APAZ) to 120–60 °C (Gleadow and Duddy, 1981; Laslett et al., 1987). The present-day surface temperature was set to 20 °C. All models are well defined since the 'goodness of fit' (GOF) values between measured and modeled data range from 0.86 to 0.97.

The so called 'lag time' (δt) is defined to integrate the time of cooling to closure temperature for the given thermochronometer, exhumation of deep seated crustal rocks to the surface, erosion, transport and finally the time of deposition (Garver et al., 1999). Differences between the closure temperature of the fission track systems and surface temperatures are much smaller when compared to other higher temperature isotopic systems. As a consequence, fission track ages will better reflect cooling processes in the shallow crustal levels (Bernet and Spiegel, 2004a,b). Furthermore, lag time is highly dependent on the wider geological context, in sense that it can be significantly shortened if the erosion, transport, and deposition occur in a tectonically active setting. In this type of settings exhumation of source areas often reflects enhanced erosion as a result of tectonically induced uplift (England and Molnar, 1990). In order to constrain the amounts and rates of exhumation/erosion for the source areas, ZFT and AFT cooling ages and modeled t-T histories are converted into rates of exhumation by using estimated (paleo)geothermal gradients.

Appendix B. Zircon U—Pb geochronology

The five rock samples (Cer1, Cer3, Cer4, Buk1, and Buk4) were crushed, sieved through 0.2 mm mesh and panned to remove the light minerals component. After that, samples were passed through Frantz isodynamic separator at 0.3 A current steps up to 1.2 A. Next step in the separation involved the use of heavy organic liquid methylene iodide (MI) of 3.325 g/cm3 density, since the zircon grains with densities between 4.6 and 4.7 g/cm3 would sink in it. Individual zircon crystals were then handpicked under microscope, placed on tape, and mounted in epoxy. Thus obtained mounts were analyzed by multicollector laser-ablation-inductively coupled plasma–mass spectrometry (LA-ICPMS) at the Arizona LaserChron Center. Following the procedures described in Gehrels et al. (2008), fragments of a large Sri Lanka zircon crystal with known age of 564 ± 4 Ma (2σ error) were used to correct for the fractionation, whereas the uncertainty resulting from the calibration correction is generally ~1% (2σ) for both $^{206}Pb/^{207}Pb$ and $^{206}Pb/^{238}U$ ages. As described in Ludwig (2005), the reported ages are determined from the weighted mean of the $^{206}Pb/^{238}U$ ages of the concordant and overlapping analyses. The reported uncertainty is based on the scatter and precision of the set of $^{206}Pb/^{238}U$ or $^{206}Pb/^{207}Pb$ ages, weighted according to their measurement errors. The standard calibration, age of the calibration standard, composition of common Pb and U decay constants, all influenced the systematic error that is ~1–2%.

References

Adam, A., Wesztergom, V., 2001. An attempt to map the depth of the electrical asthenosphere by deep magnetotelluric measurements in the Pannonian basin (Hungary). Acta Geol. Hung. 4, 167–192.

Antić, M.D., Kounov, A., Trivić, B., Wetzel, A., Peytcheva, I., Quadt, A., 2015. Alpine thermal events in the central Serbo-Macedonian Massif (southeastern Serbia). Int. J. Earth Sci.:1–21 http://dx.doi.org/10.1007/s00531-015-1266-z.

Antić, M., Peytcheva, I., von Quadt, A., Kounov, A., Trivić, B., Serafimovski, T., Tasev, G., Gerdjikov, I., Wetzel, A., 2016. Pre-Alpine evolution of a segment of the North-Gondwanan margin: geochronological and geochemical evidence from the central Serbo-Macedonian Massif. Gondwana Res. 36, 523–544.

Bada, G., Horváth, F., Dövényi, P., Szafián, P., Windhoffer, G., Cloetingh, S., 2007. Present-day stress field and tectonic inversion in the Pannonian basin. Glob. Planet. Chang. 58 (1–4), 165–180.

Balogh, K., Svingor, E., Cvetković, V., 1994. Ages and intensities of metamorphic preocesses in the Batočina area, Serbo-Macedonian Massif. Acta Mineral. Petrogr. Szeged. XXXV, 81–94.

Bennett, R.A., Hreinsdóttir, S., Buble, G., Bašic, T., Bacic, Ž., Marjanović, M., Casale, G., Gendaszek, A., Cowan, D., 2008. Eocene to present subduction of southern Adria mantle lithosphere beneath the Dinarides. Geology 36, 3–6.

Bernet, M., Spiegel, C., 2004a. In: Bernet, M., Spiegel, C. (Eds.), Introduction to Detrital Thermochronology. Geol. Soc. Am. Special Paper Vol. 378, pp. 1–6.

Bernet, M., Spiegel, C., 2004b. Detrital thermochronology—provenance analysis, exhumation, and landscape evolution of mountain belts. Geol. Soc. Am.

Bernet, M., Brandon, M.T., Garver, J.I., Molitor, B.R., 2004. In: Bernet, M., Spiegel, C. (Eds.), Fundamentals of Detrital Zircon Fission-Track Analysis for Provenance and Exhumation Studies with Examples from the European Alps. Geol. Soc. Am. Special Paper Vol. 378, pp. 25–94.

Bertotti, G., Mosca, P., Juez, J., Polino, R., Dunai, T., 2006. Oligocene to present kilometres scale subsidence and exhumation of the Ligurian Alps and the Tertiary Piedmont Basin (NW Italy) revealed by apatite (U—Th)/He thermochronology: correlation with regional tectonics. Terra Nova 18, 18–25.

Berza, T., Constantinescu, E., Vlad, S.-N., 1998. Upper Cretaceous magmatic series and associated mineralisation in the Carpathian–Balkan Orogen. Resour. Geol. 48, 291–306.

Brandon, M.T., 1992. Decomposition of fission track grain-ages distributions. Am. J. Sci. 292, 535–564.

Brandon, M.T., 2002. Decomposition of mixed grain age distributions using BINOMFIT. On Track 24, 13–18.

Brandon, M.T., Roden-Tice, M.K., Garver, J.I., 1998. Late Cenozoic exhumation of the Cascadia accretionary wedge in the Olympic Mountains, NW Washington State. Geol. Soc. Am. Bull. 110, 985–1009.

Brković, T., Radovanović, Z., Pavlović, Z., 1979. Basic geological map sheet of Yugoslavia scale 1:100.000, sheet Kragujevac L34–138. Federal Geological Institute of Yugoslavia, Beograd.

Burov, E., Yamato, P., 2008. Continental plate collision, P-T-t-z conditions and unstable vs. stable plate dynamics: insights from thermo-mechanical modelling. Lithos 103, 178–204.

Čanović, M., Kemenci, M., 1988. The Mesozoic of the Pannonian Basin in Vojvodina (Yougoslavia): Stratigraphy and Facies, Magmatism, Paleogeography. Matica Srpska, Novi Sad.

Carrapa, B., Hauer, J., Schoenbohm, L., Strecker, M.R., Schmitt, A.K., Villanueva, A., Sosa Gomez, J., 2008. Dynamics of deformation and sedimentation in the northern Sierras Pampeanas: an integrated study of the Neogene Fiambalá basin, NW Argentina. Geol. Soc. Am. Bull. 120, 1518–1543.

Carter, A., Gallager, K., 2004. Characterizing the significance of provenance on the inference of thermal history models from apatite fission-track data—a synthetic data study. Geol. Soc. Am. Spec. Pap. 378, 7–23.

Channell, J., Doglioni, C., 1994. Early Triassic paleomagnetic data from the dolomites (Italy). Tectonics 13 (1). http://dx.doi.org/10.1029/93TC01546.

Čičulić, T.M., Rakić, M., 1977. Explanatory booklet for sheet Novi Sad. (in Serbian), Basic geological map of Yugoslavia 1:100,000, (54 pp.).

Čičulić-Trifunović, M., Rakić, M., 1976. Basic geological map sheet of Yugoslavia scale 1: 100.000, sheet Novi Sad L34–100. Federal Geological Institute of Yugoslavia, Beograd.

Cvetković, V., Knezevic, M., Pecskay, Z., 2000. Tertiary Igneous Formations in the Dinarides, Vardar Zone and Adjacent Regions: From Recognition to Petrogenetic Implications. In: Karamata, S., Jankovic, S. (Eds.), Geology and Metallogeny of the Dinarides and the Vardar Zone the Academy of Science and Arts of the Republic of Srpska, Banja Luka, pp. 245–253.

Cvetkovic, V., Koroneos, A., Christofides, G., Poli, G., Knezevic, V., Eric, V., 2001. Granitoids of Mt. Cer and Mt. Bukulja and their significance for the geodynamics of the Southern Pannonian Basin. Carpathian–Balkan Geological Association XVII, Bratislava Slovakia, pp. 456–457.

Cvetković, V., Poli, G., Christofides, G., Koroneos, A., Pecskay, Z., Resimić-Šarić, K., Erić, V., 2007. The Miocene granitoid rocks of Mt. Bukulja (Central Serbia): evidence for Pannonian extension-related granitoid magmatism in the northern Dinarides. Eur. J. Mineral. 19, 513–532.

Cvetković, V., Šarić, K., Prelević, D., Genser, J., Neubauer, F., Höck, V., von Quadt, A., 2013. An anorogenic pulse in a typical orogenic setting: the geochemical and geochronological record in the east Serbian latest Cretaceous to Palaeocene alkaline rocks. Lithos 180–181, 181–199.

De Capoa, P., Di Staso, A., Giardino, S., Radoičić, R., 2002. New biostratigraphic evidences in the central-eastern belt of the Vardar Zone (Internal Dinarides). Mem. Soc. Geol. Ital. 57, 173–183.

Dimitrijević, M.D., 1997. Geology of Yugoslavia. second ed. Geoinstitute, Belgrade, Belgrade.

Dimitrijevic, M.N., Dimitrijevic, M.D., 1987. The Turbiditic Basins of Serbia. Serbian Academy of Sciences and Arts Department of Natural & Mathematical Sciences.

Djeric, N., Gerzina, N., 2008. Late Triassic radiolarians from the Ovcar-Kablar Gorge (SW Serbia). Ann. Geol. Peninsule Balkanique 69.

Djeric, N., Gerzina, N., Schmid, S.M., 2007. Age of the Jurassic Radiolarian Chert Formation from the Zlatar Mountain (SW Serbia). Ofioliti 32, 101–108.

Doglioni, C., Harabaglia, P., Merlini, S., Mongelli, F., Peccerillo, A., Piromallo, C., 1999. Orogens and slabs vs. their direction of subduction. Earth Sci. Rev. 45, 167–208.

Doglioni, C., Carminati, E., Cuffaro, M., Scrocca, D., 2007. Subduction kinematics and dynamic constraints. Earth Sci. Rev. 83, 125–175.

Dolić, D., 1997. Jezerski miocen kod Beograda. Geol. An. Balk. Poluostrva 62 (2), 15–49.

Dunkl, I., 2002. Trackkey: a Windows program for calculation and graphical presentation of fission track data. Comput. Geosci. 28 (1), 3–12.

Duretz, T., Gerya, T.V., 2013. Slab detachment during continental collision: influence of crustal rheology and interaction with lithospheric delamination. Tectonophysics 602, 124–140.

England, P., Molnar, P., 1990. Surface uplift, uplift of rocks, and exhumation of rocks. Geology 18, 1173–1177.

Erak, D., Matenco, L., Toljić, M., Stojadinović, U., Andriessen, P.A.M., Willingshofer, E., Ducea, M.N., 2016. From nappe stacking to extensional detachments at the contact between the Carpathians and Dinarides—the Jastrebac Mountains of Central Serbia. Tectonophysics (this issue).

Erdos, Z., Huismans, R.S., van der Beek, P., 2015. First-order control of syntectonic sedimentation on crustal-scale structure of mountain belts. J. Geophys. Res. Solid Earth 120, 5362–5377.

Faccenda, M., Minelli, G., Gerya, T.V., 2009. Coupled and decoupled regimes of continental collision: numerical modeling. Earth Planet. Sci. Lett. 278, 337–349.

Faccenna, C., Piromallo, C., Crespo-Blanc, A., Jolivet, L., Rosetti, F., 2004. Lateral slab deformation and the origin of the western Mediterranean arcs. Tectonics 23, TC1012 (doi: 1010.1029/2002TC001488).

Filipović, I. et al., 1971. Basic geological map sheet of Yugoslavia scale 1:100.000, sheet Vladimirci L34–124. Federal Geological Institute of Yugoslavia, Beograd.

Filipović, I., Pavlović, Z., Marković, B., Rodin, V., Marković, O., Gagić, N., Atin, B., Milićević, M., 1976. Basic geological map sheet of Yugoslavia scale 1:100.000, sheet Gornji Milanovac L34–137. Federal Geological Institute of Yugoslavia, Beograd.

Filipović, I., Rodin, V., Pavlović, Z., Marković, B., Milićević, M., Atin, B., 1979. Basic geological map sheet of Yugoslavia scale 1:100.000, sheet Obrenovac L34–125. Federal Geological Institute of Yugoslavia, Beograd.

Filipović, I., Jovanovic, D., Sudar, M., Pelikán, P., Kovac, S., Less, G., Hips, K., 2003. Comparison of the Variscan - Early Alpine evolution of the Jadar Block (NW Serbia) and "Bukkium" (NE Hungary) terranes; some paleogeographic implications. Slovak Geol. Mag. 9, 3–21.

Fodor, L., Bada, G., Csillag, G., Horvath, E., Ruszkiczay-Rüdiger, Z., Palotás, K., Síkhegyi, F., Timár, G., Cloetingh, S., Horvath, F., 2005. An outline of Neotectonic structures and morphotectonics of the Western and Central Pannonian Basin. In: Cloetingh, S., Matenco, L., Bada, G., Dinu, C., Mocanu, V. (Eds.), The Carpathians-Pannonian Basin System; Natural Laboratory for Coupled Lithospheric-Surface Processes. Tectonophysics vol. 410/1-4, pp. 15–41.

Foeken, J.P.T., 2004. Tectono-Morphology of the Ligurian Alps and Adjacent Basins (NW Italy): An Integrated Study of their Neogene to Present Evolution. (Ph.D. Thesis). VU University, Amsterdam (192 pp.).

Gallhofer, D., Quadt, A.v., Peytcheva, I., Schmid, S.M., Heinrich, C.A., 2015. Tectonic, magmatic, and metallogenic evolution of the Late Cretaceous arc in the Carpathian-Balkan orogen. Tectonics 34. http://dx.doi.org/10.1002/2015TC003834.

Garver, J.I., 2003. Etching zircon age standards for fission-track analysis. Radiat. Meas. 37 (1), 47–53.

Garver, J.I., Brandon, M.T., Rice, M.T., Kamp, P.J., 1999. Exhumation history of orogenic highlands determined by detrital fission-track thermochronology. In: Ring, U., Brandon, M.T., Willett, S.D., Lister, G.S. (Eds.), Exhumation Processes: Normal Faulting, Ductile Flow, and Erosion. Geological Society [London] Special Publication Vol. 154, pp. 283–304.

Gawlick, H.-J., Sudar, M., Suzuki, H., Deric, N., Missoni, S., Lein, R., Jovanovic, D., 2009. Upper Triassic and Middle Jurassic radiolarians from the ophiolitic mélange of the Dinaridic Ophiolite Belt, SW Serbia. N. Jb. Geol. Paläont. (Abh.) 253, 293–311.

Gehrels, G.E., Valencia, V., Ruiz, J., 2008. Enhanced precision, accuracy, efficiency, and spatial resolution of U—Pb ages by laser ablation–multicollector–inductively coupled plasma–mass spectrometry. Geochem. Geophys. Geosyst. 9, Q03017. http://dx.doi.org/10.1029/2007GC001805.

Gleadow, A.J.W., Duddy, I.R., 1981. A natural long-term track annealing experiment for apatite. Nucl. Tracks Radiat. Meas. 5, 169–174.

Green, P.F., 1985. Comparison of Zeta calibration baselines for fission-track dating of apatite, zircon and sphene. Chem. Geol. 58, 1–22.

Hatzfeld, D., Molnar, P., 2010. Comparisons of the kinematics and deep structures of the Zagros and Himalaya and of the Iranian and Tibetan plateaus and geodynamic implications. Rev. Geophys. 48, RG2005.

Horváth, F., 1995. Phases of compression during the evolution of the Pannonian basin and its bearing on hydrocarbon exploration. Mar. Pet. Geol. 12, 837–844.

Horváth, F., Musitz, B., Balázs, A., Végh, A., Uhrin, A., Nádor, A., Koroknai, B., Pap, N., Tóth, T., Wórum, G., 2015. Evolution of the Pannonian basin and its geothermal resources. Geothermics 53, 328–352.

Hrvatović, H., 2006. Geological Guidebook through Bosnia and Herzegovina. Geological Survey of Federation Bosnia and Herzegovina, Sarajevo.

Iancu, V., Berza, T., Seghedi, A., Gheuca, I., Hann, H.-P., 2005. Alpine polyphase tectonometamorphic evolution of the South Carpathians: a new overview. Tectonophysics 410, 337–365.

Jammes, S., Huismans, R.S., 2012. Structural styles of mountain building: controls of lithospheric rheologic stratification and extensional inheritance. J. Geophys. Res. Solid Earth 117.

Karamata, S., 2006. The geological development of the Balkan Peninsula related to the approach, collision and compression of Gondwanan and Eurasian Units. In: Robertson, A.H.F., Mountrakis, D. (Eds.), Tectonic Development of the Eastern Mediterranean Region. Geological Society, London, Special Publications, pp. 155–178.

Karamata, S., Stefanović, D., Krstić, B., 2003. Permian to Neogene accretion of the assemblage of geologic units presently occurring to the south of the Pannonian Basin—development of the Vardar composite terrane and adjacent units. Acta Geol. Hung. 46 (1), 63–76.

Ketcham, R.A., Donelick, R.A., Carlson, W.D., 1999. Variability of apatite fission-track annealing kinetics: III. Extrapolation to geological time scales. Am. Mineral. 84, 1235–1255.

Ketcham, R.A., Donelick, R.A., Donelick, M.B., 2003. AFT Solve: a program for multi-kinetic modeling of apatite fission-track data. Am. Mineral. 88, 929–939.

Ketcham, R.A., Donelick, R.A., Balestrieri, M.L., Zattin, M., 2009. Reproducibility of apatite fission-track length data and thermal history reconstruction. Earth Planet. Sci. Lett. 284 (3–4), 504–515.

Knežević, V., Cvetković, V., Resimić, K., 1997. Granodiorites of Stražanica on the western slopes of Cer Mt. (western Serbia). Ann. Géol. Péninsule Balkanique 61, 311–324.

Koroneos, A., Poli, G., Cvetkovic, V., Christofides, G., Krstic, D., Pecskay, Z., 2011. Petrogenetic and tectonic inferences from the study of the Mt Cer pluton (West Serbia). Geol. Mag. 148, 89–111.
Kounov, A., Seward, D., Burg, J.-P., Bernoulli, D., Ivanov, Z., Handler, R., 2010. Geochronological and structural constraints on the Cretaceous thermotectonic evolution of the Kraishte zone, western Bulgaria. Tectonics 29, TC2002.
Krstić, B., Filipović, I., Maslarević, L., Sudar, M., Ercegovac, M., 2005. Carboniferous of the central part of the Balkan Peninsula. Bull. Cl. Sci. Math. Nat. Sci. Nat. Serbian Acad. Sci. Arts 130 (43), 41–56.
Laslett, G.M., Green, P.F., Duddy, I.R., Gleadow, A.J.W., 1987. Thermal annealing of fission tracks in apatite 2: a quantitative analysis. Chem. Geol. 65, 1–13.
Lenkey, L., Dovenyi, P., Horvath, F., Cloetingh, S.A.P.L., 2002. Geothermics of the Pannonian basin and its bearing on the Neotectonics. EGU Stephan Mueller Spec. Publ. Ser. 3, 29–40.
Ludwig, K.R., 2005. User's Manual for Isoplot/Ex, Version 3.11. A Geochronological Toolkit for Microsoft Excel. Geochronology Center Special Publication, Berkeley.
Lužar-Oberiter, B., Mikes, T., Dunkl, I., Babić, L., Eynatten, H., 2012. Provenance of Cretaceous synorogenic sediments from the NW Dinarides (Croatia). Swiss J. Geosci. 105, 377–399.
Magyar, I., Radivojević, D., Sztanó, O., Synak, R., Ujszászi, K., Pócsik, M., 2013. Progradation of the paleo-Danube shelf margin across the Pannonian Basin during the Late Miocene and Early Pliocene. Glob. Planet. Chang. 103, 168–173.
Marović, M., Djoković, I., Toljić, M., Milivojević, J., Spahić, D., 2007. Paleogene-Early Miocene deformations of Bukulja-Vencac crystalline (Vardar Zone, Serbia). Ann. Geol. Peninsule Balkanique 68, 9–20.
Matenco, L., Radivojević, D., 2012. On the formation and evolution of the Pannonian Basin: constraints derived from the structure of the junction area between the Carpathians and Dinarides. Tectonics 31, TC6007.
Matenco, L., Krézsek, C., Merten, S., Schmid, S., Cloetingh, S., Andriessen, P., 2010. Characteristics of collisional orogens with low topographic build-up: an example from the Carpathians. Terra Nova 22, 155–165.
Matenco, L., Munteanu, I., ter Borgh, M., Stanica, A., Tilita, M., Lericolais, G., Dinu, C., Oaie, G., 2016. The interplay between tectonics, sediment dynamics and gateways evolution in the Danube system from the Pannonian Basin to the western Black Sea. Sci. Total Environ. 543 (Part A), 807–827.
Missoni, S., Gawlick, H.-J., Sudar, M., Jovanović, D., Lein, R., 2012. Onset and demise of the Wetterstein Carbonate Platform in the mélange areas of the Zlatibor Mountain (Sirogojno, SW Serbia). Facies 58, 95–111.
Mojsilović, S., Filipović, I., Rodin, V., Navala, M., Baklaić, D., Djoković, I., 1975. Basic geological map sheet of Yugoslavia scale 1:100.000, sheet Zvornik L34–123. Federal Geological Institute of Yugoslavia, Beograd.
Naylor, M., Sinclair, H.D., 2008. Pro- vs. retro-foreland basins. Basin Res. 20, 285–303.
Osmaston, M.F., 2008. Basal subduction tectonic erosion (STE), butter melanges, and the construction and exhumation of HP-UHP belts: the Alps example and some comparisons. Int. Geol. Rev. 50, 685–754.
Pamic, J.J., 1984. Triassic magmatism of the Dinarides in Yugoslavia. Tectonophysics 109, 273–307.
Pamić, J., 2002. The Sava-vardar Zone of the Dinarides and Hellenides versus the Vardar Ocean. Eclogae Geol. Helv. 95, 99–113.
Pavlović, Z., Marković, B., Atin, B., Dolić, D., Gagić, N., Marković, O., Dimitrijević, M.N., Vuković, M., 1979. Basic geological map sheet of Yugoslavia scale 1:100.000, sheet Smederevo L34–126. Federal Geological Institute of Yugoslavia, Beograd.
Pécskay, Z., Lexa, J., Szakács, A., Seghedi, I., Balogh, K., Konečný, V., Zelenka, T., Kovacs, M., Póka, T., Fülöp, A., Márton, E., Panaiotu, C., Cvetković, V., 2006. Geochronology of Neogene–Quaternary magmatism in the Carpathian arc and intra-Carpathian area: a review. Geol. Carpath. 57, 511–530.
Picotti, V., Pazzaglia, F.J., 2008. A new active tectonic model for the construction of the Northern Apennines mountain front near Bologna (Italy). J. Geophys. Res. 113, B08412 (doi: 08410.01029/02007jb005307).
Pinter, N., Grenerczy, G., Weber, J., Stein, S., Medak, D., 2005. The Adria Microplate: GPS Geodesy, Tectonics and Hazards (Nato Science Series: IV: Earth and Environmental Sciences). Springer.
Reiners, P.W., Brandon, M.T., 2006. Using thermochronology to understand orogenic erosion. Annu. Rev. Earth Planet. Sci. 34, 419–466 (doi: 410.1146/annurev.earth.1134.031405.125202).
Robertson, A., Karamata, S., Saric, K., 2009. Overview of ophiolites and related units in the late Palaeozoic-Early Cenozoic magmatic and tectonic development of Tethys in the northern part of the Balkan region. Lithos 108, 1–36.
Schefer, S., 2010. Tectono-Metamorphic and Magmatic Evolution of the Internal Dinarides (Kopaonik Area, Southern Serbia) and Its Significance for the Geodynamic Evolution of the Balkan Peninsula, Philosophisch-Naturwissenschaftlichen Fakultät Der Universität Basel. Universitat Basel, Basel, p. 230.
Schefer, S., Egli, D., Missoni, S., Bernoulli, D., Gawlick, H.-J., Jovanović, D., Krystyn, L., Lein, R., Schmid, S.M., Sudar, M., 2010. Triassic sediments in the internal Dinarides (Kopaonik area, southern Serbia): stratigraphy, paleogeographic and tectonic significance. Geol. Carpath. 61, 89–109.
Schefer, S., Cvetković, V., Fügenschuh, B., Kounov, A., Ovtcharova, M., Schaltegger, U., Schmid, S., 2011. Cenozoic granitoids in the Dinarides of southern Serbia: age of intrusion, isotope geochemistry, exhumation history and significance for the geodynamic evolution of the Balkan Peninsula. Int. J. Earth Sci. 100, 1181–1206.
Schmid, S., Bernoulli, D., Fügenschuh, B., Matenco, L., Schefer, S., Schuster, R., Tischler, M., Ustaszewski, K., 2008. The alpine-Carpathian-Dinaridic orogenic system: correlation and evolution of tectonic units. Swiss J. Geosci. 101, 139–183.
Schuller, V., Frisch, W., Danisik, M., Dunkl, I., Melinte, M.C., 2009. Upper Cretaceous Gosau deposits of the Apuseni Mountains (Romania) – similarities and differences to the Eastern Alps. Austrian J. Earth Sci. 102, 133–145.
Seghedi, I., Downes, H., 2011. Geochemistry and tectonic development of Cenozoic magmatism in the Carpathian–Pannonian region. Gondwana Res. 20, 655–672.
Selzer, C., Buiter, S.J.H., Pfiffner, O.A., 2008. Numerical modeling of frontal and basal accretion at collisional margins. Tectonics 27, TC3001 (doi:3010.1029/2007TC002169).
Spiegel, C., Kuhlemann, J., Dunkl, I., Frisch, W., von Eynatten, H., Balogh, K., 2000. The erosion history of the Central Alps: evidence from zircon fission track data of the foreland basin sediments. Terra Nova 12, 163–170.
Spiegel, C., Siebel, W., Kuhlemann, J., Frisch, W., 2004. Toward a comprehensive provenance analysis: a multi-method approach and its implications for the evolution of the Central Alps. Geol. Soc. Am. Spec. Pap. 378, 37–50.
Stampfli, G.M., Borel, G.D., 2002. A plate tectonic model for the Paleozoic and Mesozoic constrained by dynamic plate boundaries and restored synthetic oceanic isochrons. Earth Planet. Sci. Lett. 196, 17–33.
Stojadinovic, U., Matenco, L., Andriessen, P.A.M., Toljić, M., Foeken, J.P.T., 2013. The balance between orogenic building and subsequent extension during the Tertiary evolution of the NE Dinarides: constraints from low-temperature thermochronology. Glob. Planet. Chang. 103, 19–38.
Tagami, T., 2005. Zircon fission-track thermochronology and applications to fault studies. Low temperature thermochronology: techniques, interpretations, and applications. Rev. Mineral. Geochem. 58, 95–122.
Tari, V., 2002. Evolution of the Northern and Western Dinarides: A Tectonostratigraphic Approach. EGU Stephan Mueller Special Publications Vol. 1. European Geosciences Union, pp. 223–236.
Tari, G., Horváth, F., Rumpler, J., 1992. Styles of extension in the Pannonian basin. Tectonophysics 208, 203–219.
Tari, G., Dovenyi, P., Dunkl, I., Horvath, F., Lenkey, L., Ştefănescu, M., Szafian, P., Toth, T., 1999. Lithospheric structure of the Pannonian basin derived from seismic, gravity and geothermal data. In: Durand, B., Jolivet, L., Horvath, F., Serrane, M. (Eds.), The Mediterranean Basins: Extension within the Alpine Orogen. Geol Soc London Spec Publ Vol. 156, pp. 215–250.
ter Borgh, M., 2013. Connections between sedimentary basins during continental collision: how tectonic, surface and sedimentary processes shaped the Paratethys. Utrecht Stud. Earth Sci. 45 (212 pp.).
Toljić, M., 2006. Geological Setting of Central Vardar Zone between Avala and Kosmaj. University of Belgrade, Serbia, p. 162.
Toljić, M., Matenco, L., Ducea, M.N., Stojadinović, U., Milivojević, J., Đerić, N., 2013. The evolution of a key segment in the Europe–Adria collision: the Fruška Gora of northern Serbia. Glob. Planet. Chang. 103, 39–62.
Toljić, M., Matenco, L., Stojadinović, U., Willingshofer, E., Ljubović-Obradović, L., 2016. A forearc evolutionary model during the Cretaceous Adria–Europe convergence in the NE Dinarides. Tectonophysics (submitted for publication).
Tomljenovic, B., Csontos, L., Marton, E., Marton, P., 2008. Tectonic evolution of the northwestern internal Dinarides as constrained by structures and rotation of Medvednica Mountains, North Croatia. Geol. Soc. Lond., Spec. Publ. 298, 145–167.
Trivić, B., Cvetković, V., Smiljanić, B., Gajić, R., 2010. Deformation pattern of the Palaeozoic units of the Tethyan suture in the Central Balkan peninsula: a new insight from study of the Bukulja-Lazarevac Paleozoic unit (Serbia). Ofioliti 35 (1), 21–32.
Ustaszewski, K., Schmid, S.M., Lugovic, B., Schuster, R., Schaltegger, U., Bernoulli, D., Hottinger, L., Kounov, A., Fügenschuh, B., Schefer, S., 2009. Late Cretaceous intra-oceanic magmatism in the internal Dinarides (northern Bosnia and Herzegovina): implications for the collision of the Adriatic and European plates. Lithos 108, 106–125.
Ustaszewski, K., Kounov, A., Schmid, S.M., Schaltegger, U., Krenn, E., Frank, W., Fügenschuh, B., 2010. Evolution of the Adria-Europe plate boundary in the northern Dinarides: from continent-continent collision to back-arc extension. Tectonics 29, TC6017 (doi: 6010.1029/2010tc002668).
van Gelder, I.E., Matenco, L., Willingshofer, E., Tomljenović, B., Andriessen, P.A.M., Ducea, M.N., Beniest, A., Gruić, A., 2015. The tectonic evolution of a critical segment of the Dinarides-Alps connection: kinematic and geochronological inferences from the Medvednica Mountains, NE Croatia. Tectonics 34. http://dx.doi.org/10.1002/2015TC003937.
Vergés, J., Fernàndez, M., 2012. Tethys–Atlantic interaction along the Iberia–Africa plate boundary: the Betic–Rif orogenic system. Tectonophysics 579, 144–172.
von Eynatten, H., Dunkl, I., 2012. Assessing the sediment factory: the role of single grain analysis. Earth Sci. Rev. 115, 97–120.
von Quadt, A., Moritz, R., Peytcheva, I., Heinrich, C.A., 2005. Geochronology and geodynamics of Late Cretaceous magmatism and Cu-Au mineralization in the Panagyurishte region of the Apuseni-Banat-Timok-Srednogorie belt, Bulgaria. Ore Geol. Rev. 27, 95–126.
Wagreich, M., Faupl, P., 1994. Palaeogeography and geodynamic evolution of the Gosau Group of the Northern Calcareous Alps (late cretaceous, eastern alps, Austria). Palaeogeogr. Palaeoclimatol. Palaeoecol. 110, 235–254.
Wernicke, B., 1992. Cenozoic Extensional Tectonics of the U.S. Cordillera. In: B.C., B., Lipman, P.W., Zoback, M.L. (Eds.), The Cordilleran Orogen: Conterminous U.S.Geological Society of America, Boulder, Colorado, pp. 553–581
Willett, S.D., Brandon, M.T., 2002. On steady states in mountain belts. Geology 30, 175–178.
Willingshofer, E., Sokoutis, D., 2009. Decoupling along plate boundaries: key variable controlling the mode of deformation and the geometry of collisional mountain belts. Geology 37, 39–42.
Willingshofer, E., Neubauer, F., Cloetingh, S., 1999. The significance of Gosau-type basins for the late cretaceous tectonic history of the Alpine-Carpathian belt. Phys. Chem. Earth Solid Earth Geod. 24 (8), 687–695.
Ziegler, P.A., Cloetingh, S., 2004. Dynamic processes controlling evolution of rifted basins. Earth Sci. Rev. 64, 1–50.